Dynamic Accommodation Measurement using Purkinje Reflections and Machine Learning

by

Faik Ozan Özhan

A Dissertation Submitted to the
Graduate School of Sciences and Engineering
in Partial Fulfillment of the Requirements for
the Degree of

Master of Science

in

Electrical and Electronics Engineering

KOÇ ÜNİVERSİTESİ

May 9, 2024

Dynamic Accommodation Measurement using Purkinje Reflections and Machine Learning

Koç University

Graduate School of Sciences and Engineering

This is to certify that I have examined this copy of a master's thesis by

Faik Ozan Özhan

and have found that it is complete and satisfactory in all respects,

and that any and all revisions required by the final

examining committee have been made.

Committee Members:

____

Prof. Hakan Urey (Advisor)

____

Prof. Afsun Şahin

____

Assoc. Prof. Onur Ferhanoğlu

Date: ______________________________

ABSTRACT

Dynamic Accommodation Measurement
using Purkinje Reflections and Machine Learning

Faik Ozan Özhan

Master of Science in Electrical and Electronics Engineering
May 9, 2024

Dynamic and precise measurements of eye accommodation and vergence are important for vision research, near-eye displays (NEDs), and the diagnosis of certain visual disorders and neurological diseases. Existing biomedical devices have important limitations because they are bulky and cannot be used to accurately measure eye accommodation dynamically.

From an engineering perspective, implementing accommodation and vergence measurements in NEDs, such as augmented reality (AR) or virtual reality (VR) glasses, helps to address issues like vergence-accommodation conflict (VAC). Previous work on NEDs using adaptive focus techniques or retinal projection has reported reduced symptoms of VAC, but validating the accuracy of these systems remains challenging with current methods. Consequently, finding a simple, portable, and head-mountable method for measuring accommodation and vergence is an active area of research. There are existing approaches in the literature for measuring eye accommodation and vergence using Purkinje reflections from various layers of the eye, as well as machine learning (ML) methods. However, these methods generally do not measure accommodation but rather measure gaze and do not use all Purkinje reflections, which limits their accuracy.

In this thesis, we present a simple and efficient method for measuring accommodation and vergence using four Purkinje reflections and ML techniques, specifically multilayer perceptron (MLP) networks. We employed a ZEMAX-based eye model to simulate the positions of the Purkinje reflections at various focal distances. Despite the system's sensitivity to environmental factors, we successfully collected experimental data from nine subjects. We employed two analytical approaches to train our MLP models: subject-specific analysis using the data of individual subjects and leave-one-subject-out cross-validation (LOSO-CV) complemented by two-point calibration. To the best of our knowledge, this is the first successful implementation of the LOSO-CV method for measuring accommodation and vergence. Our system demonstrated high accuracy, predicting accommodation within 0.22 diopters (D) using subject-specific data and achieving 0.40 D accuracy with two-point calibration using data from other subjects across nine subjects.

ÖZETÇE

Purkinje Yansımaları ve Makine Öğrenimi Kullanarak Dinamik Akomodasyon Ölçümü

Faik Ozan Özhan

Elektrik ve Elektronik Mühendisliği, Yüksek Lisans

xx Mayıs 2024

Göz akomodasyonu ve verjansının dinamik ve hassas bir şekilde ölçülmesi, görme bilimi, göze yakın ekranlar (NED'ler) ve bazı görsel bozukluklar ile nörolojik hastalıkların teşhisi için önemlidir. Mevcut biyomedikal cihazların hantal olmaları gibi önemli sınırlamaları vardır ve göz akomodasyonunu dinamik olarak kesin bir biçimde ölçemezler.

Mühendislik perspektifinden bakıldığında, artırılmış gerçeklik (AR) veya sanal gerçeklik (VR) gözlükleri gibi NED'lerde akomodasyon ve verjans ölçümü, verjans-akomodasyon çatışması (VAC) gibi sorunların ele alınmasına yardımcı olur. NED'lerde adaptif odak teknikleri veya retinal projeksiyon kullanılarak yapılan önceki çalışmalar VAC semptomlarının bu çalışmalar sonucu azaldığını belirtmiştir ancak bu sonuçların kesinliğini mevcut yöntemlerle doğrulamak halihazırda zordur. Bu nedenle, akomodasyon ve verjansı ölçmek için basit, taşınabilir ve başa monte edilebilir bir yöntem geliştirmek aktif bir araştırma alanıdır. Literatürde, gözün çeşitli katmanlarından Purkinje yansımalarını ve makine öğrenimi (ML) yöntemlerini kullanarak göz akomodasyonu ve verjansı ölçmek için yöntemler vardır. Ancak, bu yöntemler esas olarak akomodasyonu değil, daha çok bakış açısını ölçerler ve tüm Purkinje yansımalarını kullanmazlar, bu da bu sistemlerin doğruluklarını sınırlar.

Bu tezde, dört Purkinje yansıması ve ML tekniklerini, özellikle çok katmanlı algılayıcı (MLP) ağlarını kullanarak akomodasyon ve verjansı ölçmek için basit ve etkili bir yöntem sunuyoruz. Çeşitli odak uzaklıklarında Purkinje yansımalarının pozisyonlarını simüle etmek için ZEMAX tabanlı bir göz modeli kullanıdk. Sistemin çevresel faktörlere duyarlılığına rağmen, dokuz katılımcıdan başarılı bir şekilde deneysel veri topladık. MLP modellerimizi eğitmek için iki farklı analitik yönteme başvurduk. Bunlar bireylerin kendi verilerini kullanarak yaptığımız bireysel analiz ve iki noktalı kalibrasyonla tamamlanan bir katılımcıyı dışarıda bırakma çapraz doğrulamasıydı (LOSO-CV). Bildiğimiz kadarıyla bu çalışma akomodasyon ve verjansı ölçmek için LOSO-CV yönteminin başarılı bir şekilde uygulandığı ilk çalışmadır. Sistemimiz yüksek doğrulukta çalışmıştır. Bireysel veriler kullanarak akomodasyon 0.22 diyoptri (D) doğrulukla tahmin edilebilmiş ve diğer katılımcıların verilerinin kullanıldığı iki noktalı kalibrasyonla tamamlanan metodla dokuz katılımcı arasında 0.40 D doğruluk elde edilmiştir.

ACKNOWLEDGEMENTS

I would like to express my appreciation to my MSc supervisor, Prof. Hakan Ürey, for his guidance and support during my MSc studies. His experience and enthusiasm for research were invaluable, significantly inspiring me to develop an academic stance and intellectual perspective throughout the process.

I would also like to thank Prof. Afsun Şahin for his beneficial assessment of my thesis work from a clinical perspective and for the insightful feedback he provided in this regard.

Additionally, I express gratitude to the thesis defense committee members, Prof. Hakan Ürey, Prof. Afsun Şahin, and Assoc. Prof. Onur Ferhanoğlu for dedicating their valuable time and contributing to the evaluation process.

I sincerely thank the present and past members of OML. Specifically, I would like to acknowledge the invaluable support and significant contributions made by Dr. Uğur Aygün and Dr. Parviz Zolfaghari to my research.

I extend my deepest gratitude to my parents, Özgür and Mehmet Özhan, for their support, love, and understanding. Their support has been my greatest fortune, especially in overcoming the challenges faced throughout this journey. Special thanks to my friends Dilara Saçal, Günce, Gündüz, Barış Can Okur, Alkım Akman, Onur Doğan, Uğur Karataş, and Şilan Töre İnce, for always being there during my lows and effortlessly boosting my spirits. Last, I am particularly grateful to Mustafa Malkoç, whose belief in and support for me have remained constant under all circumstances. This thesis would not have been possible without your invaluable contributions.

TABLE OF CONTENTS

LIST OF TABLES

LIST OF FIGURES

ABBREVIATIONS

MLP	Multilayer Perceptron
NED	Near-Eye Display
RMSE	Root Mean Square Error
MSE	Mean Square Error
VAC	Vergence-Accommodation Conflict
D	Diopters
LOSO-CV	Leave-One-Subject-Out Cross-Validation
CF1	Configuration 1
CF2	Configuration 2
ML	Machine Learning
AR	Augmented Reality
VR	Virtual Reality
R^2	Coefficient of Determination
r	Pearson Correlation Coefficient

Chapter 1:
BACKGROUND

This chapter offers essential background information that will enhance the reader's understanding of the thesis. It introduces two critical concepts related to depth perception: accommodation and vergence. The chapter explains the mechanisms behind these concepts and explores the relationships among them.

1.1 *Eye Accommodation*

1.1.1 Definition

Our eye adjusts its optics when we look at objects at different distances. This ensures clear vision, and it is crucial for navigating daily activities. This optical adjustment is named eye accommodation and refers to the capacity of the human eye to adjust its optical power and shift its focus from distant objects to those that are closer. Optical power is the ability of the eye to refract light rays and focus them onto the retina. The accommodation process occurs through a series of complex mechanisms aimed at producing sharp and focused images [1]. Primarily, the shape of the human crystalline lens changes during the accommodation process, resulting in a change in optical power [2]. Accommodation is a closed-loop process that generates negative feedback. Therefore, the accommodation process continues until a clear, nonblurred image is produced. The accommodation distance is defined as the distance between the eye of the observer and the object in focus and is measured in terms of diopters (D).

1.1.2 Accommodation process

When eye accommodation changes, the optical power of the eye increases or decreases. Although the sympathetic nervous system is involved in the accommodation process, it is mostly driven by the parasympathetic nervous system [3], so it can be considered a reflex. The widely accepted and still predominant theory proposed by Helmholtz explains this phenomenon. The main eye components that play a role in the accommodation process are the ciliary muscles and crystalline lens. The shape of the human crystalline lens is affected by the force exerted on the lens by ciliary muscles [4, 5]. The accommodation process is visualized in Figure 1.1, which is adapted from [6].

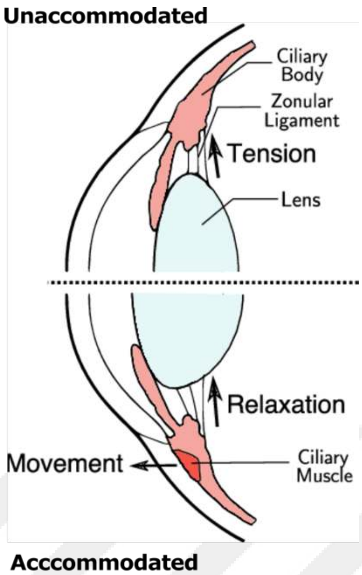

Figure 1.1: Visualization of the accommodation process. Adapted from [6].

When we shift our gaze from a distant object to a nearer object, the ciliary muscles contract. This contraction moves the choroid forward and relaxes the zonules. This puts the crystalline lens into a more convex shape and increases its refractive power. Thus, rays of light coming from nearby objects are accurately focused onto the retina. In the reverse scenario, the focus point shifts from near to distant, resulting in ciliary muscle relaxation. This relaxation pulls the choroid to the back side and stretches the zonules, resulting in a more concave lens [4, 7, 8]. In conclusion, it can be said that the ciliary muscles do all the work in the accommodation process.

Even if the ciliary muscles are activated during the accommodation process, there are some cues that trigger the process. The most important cue for accommodation is the blurry retinal image caused by defocus blur and optical aberrations of the human eye. Second, proximity cues related to the perceived distance of objects contribute to driving accommodation. Last, the cues that drive vergence also influence accommodation due to the vergence-accommodation cross-link. We will discuss vergence and this cross-link in more detail in the following sections.

1.2 Vergence

Before exploring the details of the vergence process, it is essential to first understand the concept of binocular vision. Binocular vision is the ability to perceive the world as a single clear image with two eyes. The images captured by the eyes differ slightly from each other since they are viewed from different perspectives. This phenomenon is known as binocular disparity. The brain processes the overlapping areas of retinal images to create a single, expanded field of view (FOV), which is larger than that of monocular vision [9]. The combined use of both eyes enhances spatial perception, depth perception, and overall visual performance and enables the perception of three-dimensional space [10].

During binocular accommodation, while we shift our gaze from one object to another, the eyes are moving with the gaze. As a result, our eyes fixate upon the gaze point, and this process is known as vergence. Vergence can occur whether one is transitioning one’s gaze from near to far distances or from far to near distances. Convergence is the way our eyes move together and point inward when we look at nearby objects [11]. The opposite is called divergence, which is the movement of the eyes when we shift our focus from a near object to a distant one. The amount of rotation is defined as the vergence angle and is measured in terms of degrees.

1.3 Vergence–Accommodation Interaction

Vergence and accommodation are closely linked, as any change in one directly affects the other due to the crosslink between them in our brain's visual system. In this subsection, we will discuss two mechanisms: one explains how they are coupled, and the other describes the conditions under which mismatches occur.

1.3.1 Vergence-Accommodation Cross-link

The accommodation-vergence cross-link defines the coordinated interactions between the binocular accommodation and vergence systems. It is driven by cues such as blur and disparity, and it ensures a single, clear vision at different distances. [9]. Schor proposed a cross-coupling model between vergence and accommodation to explain how these cues affect accommodation and vergence [12]. As we mentioned previously, the main cue for accommodation is the blurry image formed on the retina. However, this assumption is valid only when accommodation is stable and is the only task sustaining the current accommodative state. If the accommodation dynamically changes from one point to another, then the vergence-driven binocular disparity cue becomes the dominant factor triggering accommodation. This same effect is interchangeably valid for vergence. This cross-linking mechanism helps accommodation and vergence to follow each other and helps preserve clear and single vision.

1.3.2 Vergence-Accommodation Conflict

The vergence accommodation conflict (VAC) arises when the neural coupling between vergence and accommodation becomes mismatched [13]. In binocular vision, when we focus on targets at some distance, our eyes must converge to focus on the same point. This distance is called the vergence distance, and the eyes adapt the accommodation to that certain spot to obtain a sharp image. Since the mechanisms are neutrally coupled, if there is any change in the vergence angle, the eye accommodates at a certain distance. When the vergence distance and the accommodative distance are not accurately matched, this conflict can lead to visual discomfort and fatigue [14, 15]. This conflict is particularly evident in stereoscopic 3D displays, where the right and left eyes receive different images. This causes variations in binocular disparities as the viewer observes the 3D content [16]. While the eyes converge to perceive depth, the plane of focus remains fixed on the display screen, disrupting the natural correlation between vergence and accommodation. Consequently, users may experience discomfort due to the VAC induced by the disparity between convergence and accommodation cues [17].

1.4 Purkinje Reflections

Purkinje reflections (or images) are reflections from various layers of the eye. These reflections are named by the Czech scientist who discovered them, Jan Evangelista Purkyně, in 1823. There are four main Purkinje reflections that can be easily formed by a light source and captured by a camera. The first Purkinje reflection (P1) is formed by the anterior surface of the cornea, and this is the brightest spot, as expected. The second Purkinje reflection (P2) is from the posterior surface of the cornea, whose brightness is less than that of the first Purkinje image but still bright. The first and second Purkinje images generally cannot be separated when we capture them through a camera since they are formed very close to each other. The third Purkinje reflection (P3) formed from the anterior surface of the crystalline lens, and the fourth Purkinje reflection (P4) formed from the posterior surface of the human crystalline lens. There are also higher-order Purkinje reflections that may be observable in some cases, but they are generally not considered in modern applications. Figure 1.2 illustrates the formation of the four Purkinje images through ZEMAX simulations in sequential mode. For enhanced visualization, the formation of P1 and P2 is depicted in Figure 1.2a, whereas the formation of P3 and P4 is presented in Figure 1.2b.

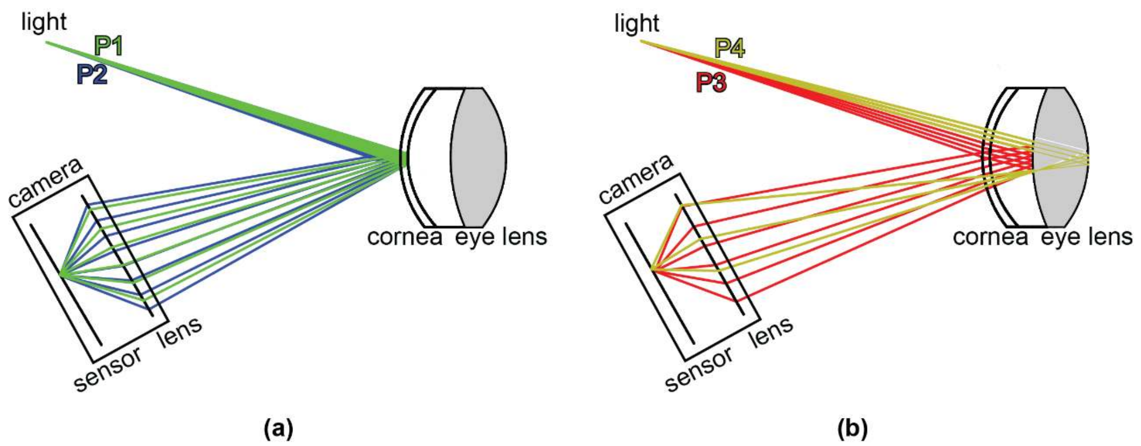

Figure 1.2: Illustration of the formation of the Purkinje images (a) P1 and P2 (b) P3 and P4 through ZEMAX simulations in sequential mode (adapted from [18]).

The four main Purkinje reflections utilized in various applications include the decentration of the intraocular lens during cataract or refractive surgery [19], the assessment of the density and transmittance of the human crystalline lens [20], and a wide range of gaze tracking [21].

Purkinje reflections have also been utilized for measuring accommodation and vergence. Considering that the shape of the crystalline lens varies with accommodation, we can say that the positions of the P3 and P4 reflections change accordingly. Conversely, vergence affects the positions of all Purkinje images as the eye rotates during the vergence process. If a relationship between accommodation, vergence, and the change in Purkinje reflections is established, it could be possible to predict the accommodation distance and vergence angle accurately.

This concept builds on early methods that extensively utilized Purkinje reflections for eye tracking, which were later adapted for accommodation and vergence prediction [22, 23]. This adaptation was primarily initiated by recent advancements in applications of ML and DL techniques that inspired vision scientists to explore the possibility of predicting accommodation and vergence based on Purkinje reflections. Various kinds of eye trackers that can measure accommodation have been developed [24, 25, 26]. However, the prediction accuracy of these methods is limited since they use either P1&2 and P3 (discarding P4) or P1&2 and P4 (discarding P3) as inputs for their model.

1.5 Contribution of the thesis

In this thesis, we developed a simple and efficient method for measuring accommodation and vergence using Purkinje reflections and machine learning. Our setup consists of one NIR camera and one NIR LED source for one eye, offering a very simple, efficient, and head-mountable method for measuring accommodation and vergence.

Contrary to previous approaches, our method uses all four Purkinje images to make predictions. Data from 9 subjects were collected for this purpose, and analyses were performed on these data. We primarily employed three different analysis schemes for our method: feature-based correlation analysis, subject-specific MLP analysis, and leave-one-subject-out cross-validation-based MLP analysis. To our knowledge, this thesis is the first to implement the leave-one-subject-out cross-validation method within the accommodation context. We evaluated the system performance using two different sets of input parameters, which allowed us to understand the effect of pupil size on the results.

We demonstrated that using Purkinje reflection coordinates in machine learning results in precise estimations to some extent. The proposed system accurately predicted accommodation with an accuracy better than 0.22 Diopters (D) using the subject's own data and 0.40 D using data from other subjects with two-point calibration in tests performed with nine subjects in our setup. Finally, we determined the effect of each parameter on the predictions using the feature importance technique, which provides insight into which parameter is important for accommodation prediction and which is important for vergence.

Chapter 2:
DYNAMIC ACCOMMODATION MEASUREMENT USING PURKINJE REFLECTIONS AND MACHINE LEARNING

Adapted from reference [18], Faik Ozan Ozhan, Ugur Aygun, Afsun Sahin, Hakan Urey, Dynamic accommodation measurement using Purkinje reflections and machine learning.

2.1 Introduction

Eye movements are fundamental for the proper functioning of the visual system. One group of these movements we experience appears when our eyes converge to focus on a specific point in space, which was stated in section 1.2. The measurement of eye movements, especially vergence, is significant in the diagnosis and management of neurological diseases such as multiple sclerosis [27, 28] and Parkinson’s disease [29, 30] or vision disorders such as strabismus [31, 32], nystagmus [33, 34, 35], amblyopia [31, 36, 37], and achromatopsia [38]. Furthermore, the exact measurement of accommodation, the function of the eye to focus, is critical for answering many questions related to refractive errors and the refractive state of the eye [39, 40, 41]. Therefore, advanced biomedical devices have been developed to measure the accommodative properties and vergence ability of the eye in clinical settings, which contributes to the understanding and treatment of a variety of dysfunctions.

The implementation of accommodation and vergence measurements in near-eye displays (NEDs), such as augmented reality (AR) or virtual reality (VR) displays, has the potential to provide solutions to issues like the vergence-accommodation conflict (VAC) mentioned in subsection 1.3.2. Prior work on NEDs with adaptive focus techniques or retinal projection has reported lower symptoms of VAC [42], and its effects on various tasks have been analyzed in different studies [43, 44, 45, 46]. Such systems automatically adjust their focus to the stereoscopic distance, allowing for the perception of the proper depth and detail, which creates a more realistic user experience. The measurement of stereoscopic distance and vergence with high accuracy is possible using different technologies, such as eye tracking, which has been widely investigated for a long time.

Eye tracking technologies are first embedded into clinical tools or AR/VR display units to track and record user gaze and vergence. Then, the recorded data are used to update the focus (and thus the virtual distance) within these technologies. Nevertheless, the effectiveness of these systems must be quantified and confirmed in ways that can objectively measure the accommodation induced by the system. Autorefractors meet this need and have been used throughout this validation process.

Autorefractors are very common devices in ophthalmology clinics and are used to assess refractive errors in patients before a comprehensive eye examination is performed [47, 48, 49]. Their working principle takes advantage of the refractive properties of the eye and is mainly based on sending a light beam into the eye and observing its reflection off the retina. Although their main task is to measure refractive errors, some open field autorefractors also have the ability to assess dynamic accommodation, which is not a common feature. However, most currently available autorefractors are not portable, which makes them inconvenient for tracking accommodation during daily activities or for integration with head-mounted devices. Recently, a few brand-new open-view autorefractors suitable for commercial and portable use have emerged, but dynamic accommodation measurement is not considered one of their capabilities. Therefore, finding a way to measure accommodation precisely in a low-cost and efficient manner remains an active area of research.

Methods can be developed to estimate the accommodation depth and vergence angle from the locations of Purkinje reflections captured through the camera. In this thesis, we explored the possibility of using all Purkinje reflections to measure accommodation and vergence, contributing to the literature.

2.2 *Methods*

This chapter focuses on the optical setup, components, data collection and analysis, and the utilized measurement or prediction methods. The overall system was constructed on an optical bench at the Koç University Optical Microsystems Laboratory.

2.2.1 Experimental Design and Setup

In this subsection, the details of the experimental setup developed to measure vergence and accommodation using Purkinje reflections are provided. The fundamental aspect of the setup was its ability to capture Purkinje images. Thus, the necessary components were determined for their formation and observation before the construction of the optical setup. One camera and a suitable light source are sufficient for observing Purkinje images. However, their specifications affect the quality of observations and should be determined considering several factors. First, the light source should not cause ocular discomfort and should effectively facilitate the formation of Purkinje images. In addition, this source should be considered eye-safe and invisible to the human eye to properly conduct experiments. An NIR LED source (TSAL6200, Vishay Intertechnology, Inc.) with a peak wavelength of 940 nm was chosen to meet these criteria.

The following stage of the optical design was to capture the Purkinje reflections effectively. This requires a camera that is compatible with a 940 nm wavelength and small enough to not obstruct the human visual field when it is placed near the eye. As an extra feature, the camera should have a focus adjustment capability to focus on the eye surface from short distances with no additional lenses. An NIR camera (SQ11 Mini DV Camera, Dilwe1) was selected based on these specifications.

The next step was determining the component that represented the target points corresponding to certain locations in 3D space to induce the accommodation of the subjects at a certain time. This component was chosen based on the following design criteria. The targets should not occlude each other, can be seen clearly and receive subjects' attention. In addition, automation of switching from one target to another allows experiments to be executed quickly and effectively without the need for direct instructions. Overall, we employed a commercial WS2812B smart control RGB light source array from the WorldSemi LED Company and programmed the LEDs on it as target points. Switching on the specific LED that participants were intended to look at was a clear guide for the implementation of the experiment. The LEDs were dimmed to the brightness level that the subject could accommodate without any disturbance. The color of the LEDs was chosen based on two facts. First, the human eye's response to red light is shorter than that to other visible wavelengths. Second, according to a recent study [52], all colors similarly trigger accommodations. Therefore, red LEDs operating at 620 nm were selected for the experiments.

The placement of the components relative to the eye is as important as their selection. The positions of the two NIR LED sources and two NIR cameras (one of each for each eye) were adjusted and fixed according to each other by making use that all Purkinje images were present in the image for all different target points, and they did not coincide. The RGB light source array was not fixed, and its position was changed for various applications, unlike those of cameras and LEDs. However, its length is set to cover the distance range over which the experiments will be performed, from 4 D (selected since it represents the minimum distance that an adult with healthy eyes can focus) to 1 D (chosen due to space constraints). In the first configuration (CF1), the RGB LED array was positioned along either the visual axis of the right eye or the left eye. This made it possible to observe only the effect of monocular accommodation on Purkinje reflections since the eye, whose visual axis aligns with the RGB LED array, does not rotate while the subject is looking at target points. However, the target LEDs should not occlude each other, particularly for the eye, which does not rotate. Thus, it was ensured that there was no occlusion and that all light sources were easily observable to the human eye by positioning the RGB LED array at a very small angle in the vertical direction. The impact of this angle on the results was negligible because it was extremely small. Second, the RGB light source array was positioned along the midline between the visual axes of the eyes to observe changes in Purkinje reflections with combined accommodation and vergence effects. In this second configuration (CF2), the eye rotates to fixate and accommodate upon a target point; thus, the vergence effect is also involved. The angle of rotation was determined using Equation 2.1, where d_{target} represents the minimum distance between the eye's visual axis and the target point, and d represents the subject's minimum distance from the target point:

$$\theta = \arctan\left(\frac{d_{target}}{d}\right) \tag{2.1}$$

In conclusion, two configurations were present in our experiments: one demonstrated only the accommodation effect on Purkinje reflections, while the other showed the combined effects of vergence and accommodation.

2.2.2 ZEMAX Simulations

ZEMAX ray tracing simulations were conducted to understand the formation of Purkinje reflections prior to conducting the experiments. Before the simulations, the operational mode should be set, and the model should be constructed. Among the two different operational modes of ZEMAX, the nonsequential mode enables light to travel along optical elements without restrictions. This made it a proper choice since the light should reflect off from different layers of the eye in our proposed model. Next, the fundamental components of our experimental setup, including the camera, LED and eye, are modeled. Figure 2.1 shows a 3D representation of our model and the corresponding section of the experimental setup for comparison.

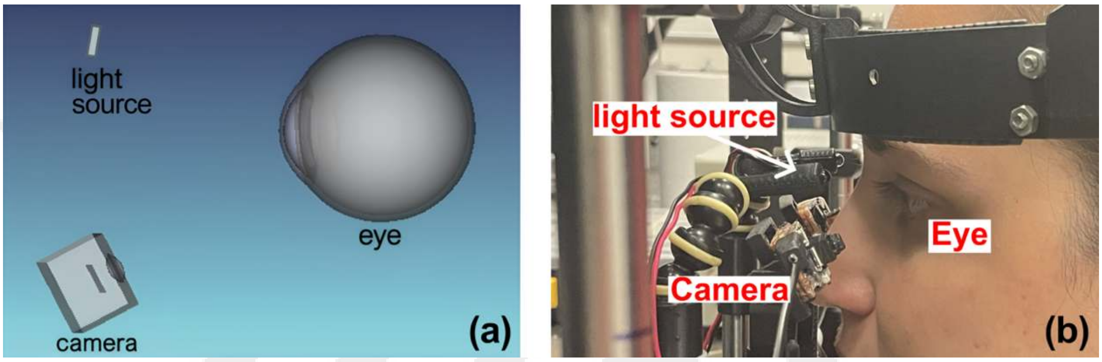

Figure 2.1: (a) 3D representation of our model and (b) corresponding section of the experimental setup.

The camera and LED were characterized through a lens data editor in ZEMAX, considering their specifications. These specifications can be listed as the peak wavelength, spatial radiation pattern, and beam angle for the LED, while the sensor size, resolution, f-stop number, and focal length apply to the camera. However, for the sake of simplicity, it was not necessary to precisely implement these specifications during modeling since our main purpose was to find the range of optimum locations of the components. Taking this into account, the LED was modeled as a radial source with a beam angle of 30 degrees, and the NIR camera was modeled as a detector rectangle with a simple detector in front. On the other hand, we accurately modeled the eye, particularly its surface parameters, as they have a significant effect on the locations of Purkinje images. Our eye model was built upon Navarro's eye model [50], except for the constant pupil size of 4 mm during the simulations. This model incorporates the inner and outer surfaces of the cornea and eye lens, which makes it appropriate for simulating Purkinje images. In addition, the model parameters are expressed as a function of the accommodation distance, which enables us to simulate focus changes more easily.

However, the only drawback of the model is that the refractive indices of ocular media are determined only for certain wavelengths. Therefore, the refractive indices were modified using Herzberger's formulas [51] to account for a wavelength of 940 nm, which is the peak wavelength of the LED. The resulting parameters used for constructing the eye model are given in Table 2.1.

Table 2.1: Model Eye Parameters. The accommodation is denoted as A (in Diopters). Model parameters are based on Navarro's eye model [50]. Refractive indices were modified for the NIR LED used in our experiments.

Parameters	Value
Radius of curvature (mm)	
Anterior surface of cornea	7.72
Posterior surface of cornea	6.5
Anterior surface of lens	$10.2 - 1.75 \cdot \ln(A + 1)$
Posterior surface lens	$-6 + 0.2294 \cdot \ln(A + 1)$
Surface Thickness (mm)	
Cornea	0.55
Aqueous	$3.05 - 0.05 \cdot \ln(A + 1)$
Lens	$4 + 0.1 \cdot \ln(A + 1)$
Vitreous	$16.4 - 0.05 \cdot \ln(A + 1)$
Asphericity	
Anterior surface of cornea	-0.26
Posterior surface of cornea	0
Anterior surface lens	$-3.1316 - 0.34 \cdot \ln(A + 1)$
Posterior surface lens	$-1 - 0.125 \cdot \ln(A + 1)$
Refractive index (at 940 nm)	
Cornea	1.368
Aqueous	1.3293
Lens	$1.41157 + 8.0064 \cdot 10^{-5} \cdot (10 \cdot A + A^2)$
Vitreous	1.329

Using Table 1, the parameters were changed to make focus adjustments while keeping the axial length constant. Eye rotation was also modeled to take vergence into account by changing the location parameters. Figure 2.2 provides the preliminary simulation results, which demonstrate the chief rays of Purkinje reflections for four different target points, as shown in the small insets to the right of each subfigure. The optical path in the subfigures indicates the top view of the target point and the eye directed toward it. The camera was not included in these simulations since only chief ray analysis was performed. It can be deduced that the maximum change occurs in P3 as accommodation changes. On the other hand, vergence significantly changes the direction of P4, which is expected given that P4 is formed from reflections off the maximum number of layers.

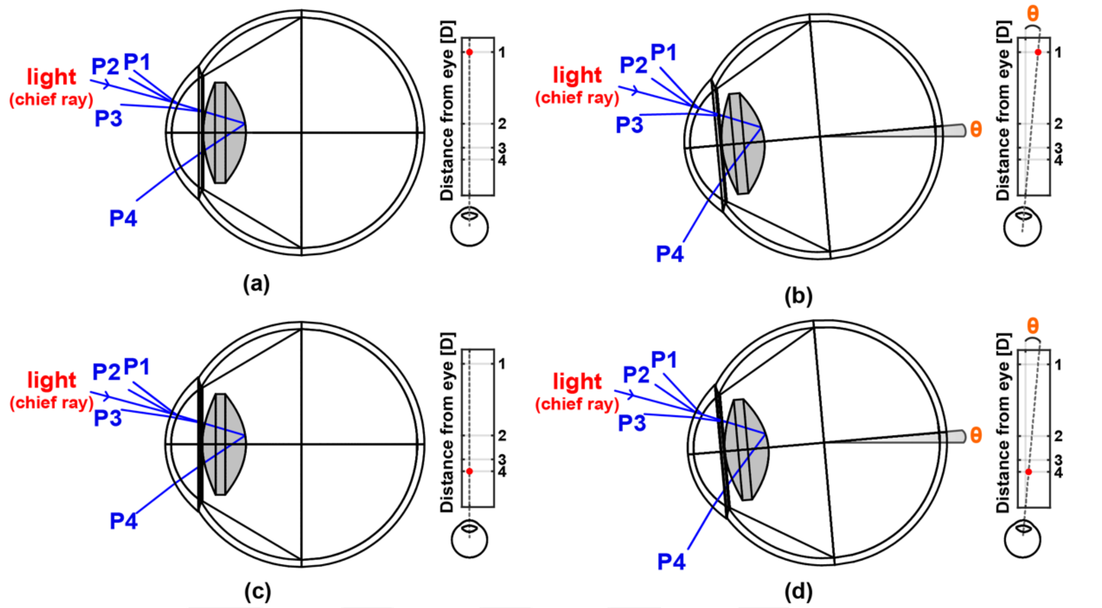

Figure 2.2: Preliminary results demonstrating the chief rays of Purkinje reflections for different target positions. (a) Accommodation and vergence at 1 D and 0 deg. (no eye rotation), (b) accommodation and vergence at 1 D and 5 deg., (c) accommodation and vergence at 4 D and 0 deg. (no eye rotation), and (d) Accommodation and vergence at 4 D and 5 deg.

After constructing the model, the ZEMAX programming language was used to automate the process of changing the locations of the LED and camera. This automation involved looping through various combinations within a predetermined range of positions for these components. The extremes of CF1 and CF2 correspond to four target points (4 D and 1 D accommodations in each configuration), which are simulated for each combination to assess how each configuration affects the results. We used the detector viewer tool to analyze the results for each combination by saving the ray trace results as image files on a detector rectangle, which is part of our camera model. The saved images are then postprocessed to determine the locations of Purkinje reflections. As a final note, all the simulations were performed with ZEMAX OpticStudio version 19.4 SP1. The images were processed with Python version 3.11.2.

2.2.3 Data Collection

After positioning all the components, the data collection procedure was established as explained in this subsection. The target points were identified as a part of the data collection scheme. We set the target points from 4 D to 1 D with 0.5 D intervals, which is double the minimum detectable accommodation change by young adults with healthy eyes. Next, the individual LEDs at these 0.5 D intervals were identified as our target points. For this purpose, one end of the RGB LED array was positioned 4 D (25 cm) from the eye. Then, the distance between individual LED light sources was measured as 16.6 mm. LED indices corresponding to each distance at 0.5 D intervals between 4 and 1 D were identified. Following this, the duration for the subjects to look at each target was determined to be 2 seconds, which is much greater than the time required for the subjects to change focus from one target to another. Finally, we specified the order of the target points from 4 D to 1 D in descending order in terms of diopters. Overall, custom code for a microcontroller (Arduino Uno) is written to control an RGB LED array based on the serial data received. The LEDs corresponding to the target distances were switched on and off sequentially through serial commands sent from a custom Python script to the microcontroller.

The next step in the data collection procedure was placing the subjects into the setup quickly and efficiently since the Purkinje images are very sensitive to head movements. Therefore, the subjects placed their heads on the headrest and chinrest according to the following instructions after a monitor in which the camera stream was displayed was mounted in front of the setup. The subjects were guided to look at a specific part of the screen and move their heads around until their pupil entered the desired region. Piezo stages, which change the positions of the camera and NIR LED to the same extent, were utilized for the cases in which the subjects could not position their heads appropriately. These piezo stages were also employed when the subjects' interpupillary distances were at the extremes. Following subject recruitment, the eye from which the data will be collected will be determined, and the corresponding camera will be activated. The various image frames captured through the camera during this process are shown in Figure 2.3.

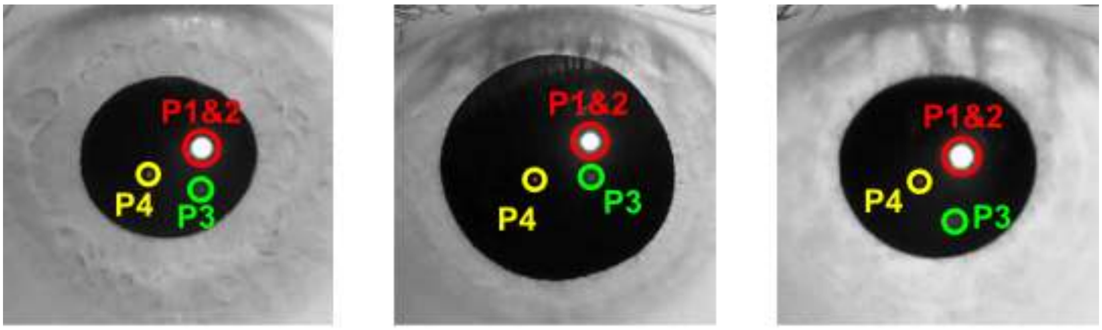

Figure 2.3: Preliminary results showing the Purkinje reflection locations captured through the camera corresponding to the left eye.

The data collection started with CF1, in which the RGB LED array was positioned along the visual axis of the eye of interest. The LED that corresponds to the target distance was switched on, and the images were captured and recorded through the camera working at 50 Hz. This automation was facilitated by a custom-written Python script that sends commands to the microcontroller to turn on the LED, activate the camera, and capture the data.

Considering that the subjects focused on each target for a duration of 2 seconds and that the camera operated at a speed of 50 Hz, 100 image frames for each target point were captured and recorded. In total, 1400 frames were obtained from 7 different target points for CF1. Then, the same procedure was applied for CF2. In conclusion, 2800 images were obtained through a single run of data collection procedure. Figure 2.4 shows our experimental setup schematics for CF1 and CF2 along with images of the setup.

The data were collected from the left eyes of 9 healthy adults with no other eye diseases except for refractive errors. Two subjects were recruited for additional experiments to investigate the effects of several factors on the measurements. To investigate the effect of interocular variability, data were collected from the right eyes of the subjects underwent the normal procedure. To investigate whether habituation to recurrent simulation affects the data, the left eyes of the participants were subjected to a randomized data collection procedure. In this approach, the LEDs corresponding to target points within each configuration were randomized among themselves. Finally, the repeatability of the measurements was tested by replicating experiments for these 2 subjects and calculating the Pearson correlation coefficient and p-value.

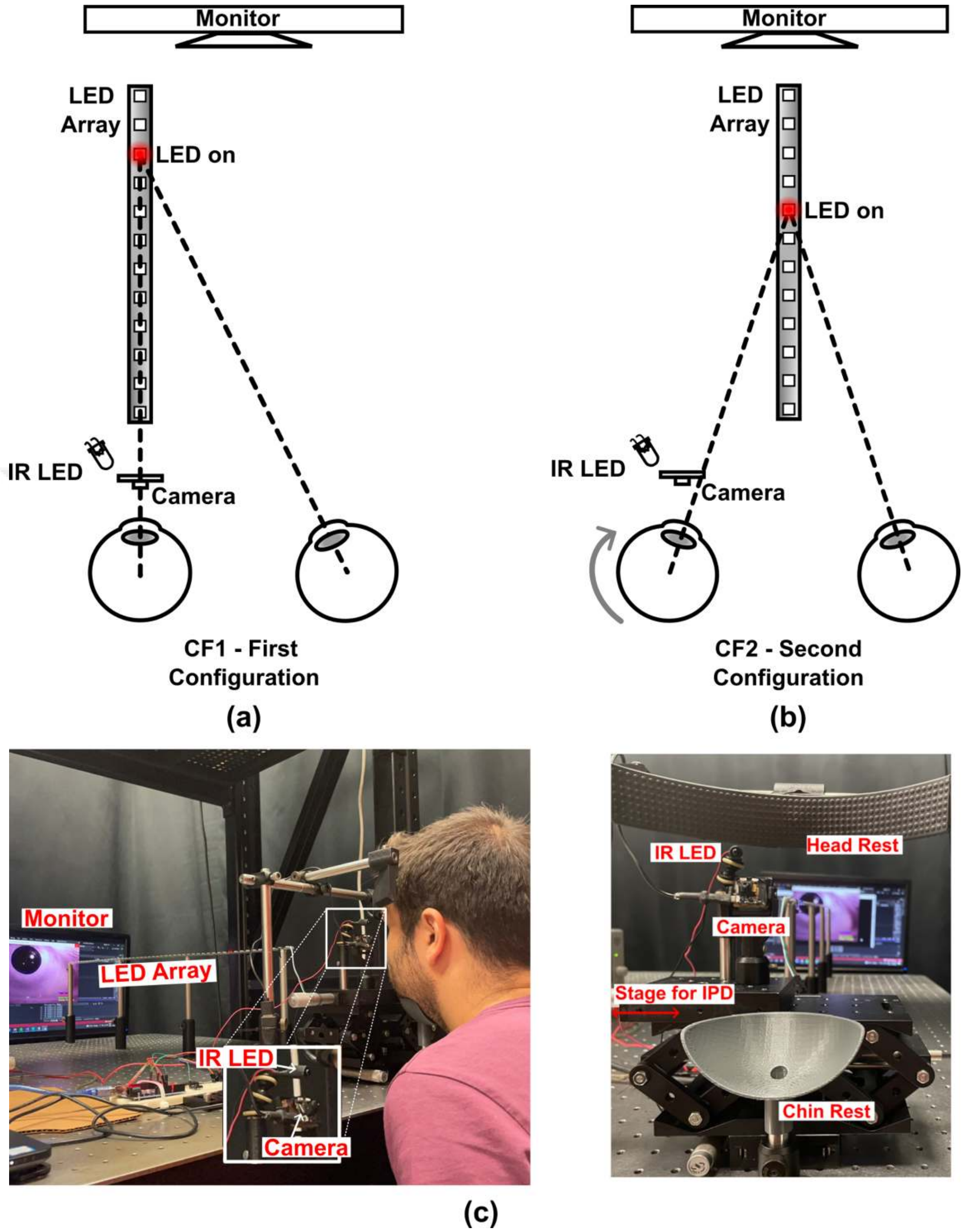

Figure 2.4: Setup schematics showing different configurations (a) CF1, for observing only the accommodation effect, and (b) CF2, for observing the combined effects of accommodation and vergence on Purkinje reflections. (c) Pictures of the experimental setup.

2.2.4 *Data Analysis Methodology*

In this subsection, the data analysis methodology is explained from finding the locations of Purkinje reflections via image processing algorithms to estimate the accommodation and vergence via ML methods. First, the reaction time—the amount of time it takes for the visual system to react to a visual stimulus—was considered. Since our data collection immediately started after the activation of the LED, which represented the current target point, some frames were captured before the eye responded and accommodated to it. Therefore, we discarded these frames before proceeding.

Image Processing Algorithm

The remaining frames were processed to determine the locations of the Purkinje reflections and the pupil parameters. Conventional image processing techniques were implemented using the OpenCV library in Python for this purpose. The algorithm involves many steps, so only the main points are detailed in this thesis. First, the image was converted to grayscale, and Gaussian blurring was applied to reduce the noise. It was then transformed into a binary image. The pupil region was identified by employing a contour detection method, selecting the largest contour, and fitting an ellipse around it. On the other hand, the blob detection method was employed to detect P1. In this method, the regions in the binary image were analyzed based on predetermined parameters that are different for P1 compared to the other candidate points. The center of the region that satisfied this parameter-based selection criterion was chosen as P1.

Upon finding the best fitted ellipse to the pupil region and the location of P1, the next step was to determine the locations of P3 and P4. Since P3 and P4 should lie inside the pupil, the original image was cropped as a rectangle that encompasses the pupil region first. Adaptive histogram equalization was then applied to increase contrast without increasing the noise level, which made P3 and P4 more prominent relative to their surroundings. Adaptive thresholding was applied to contrast-enhanced images to obtain a few candidate areas for P3 and P4. Finally, the blob detection method was used to detect P3 and P4 among the candidate regions. Our image processing scheme is shown in Figure 2.5.

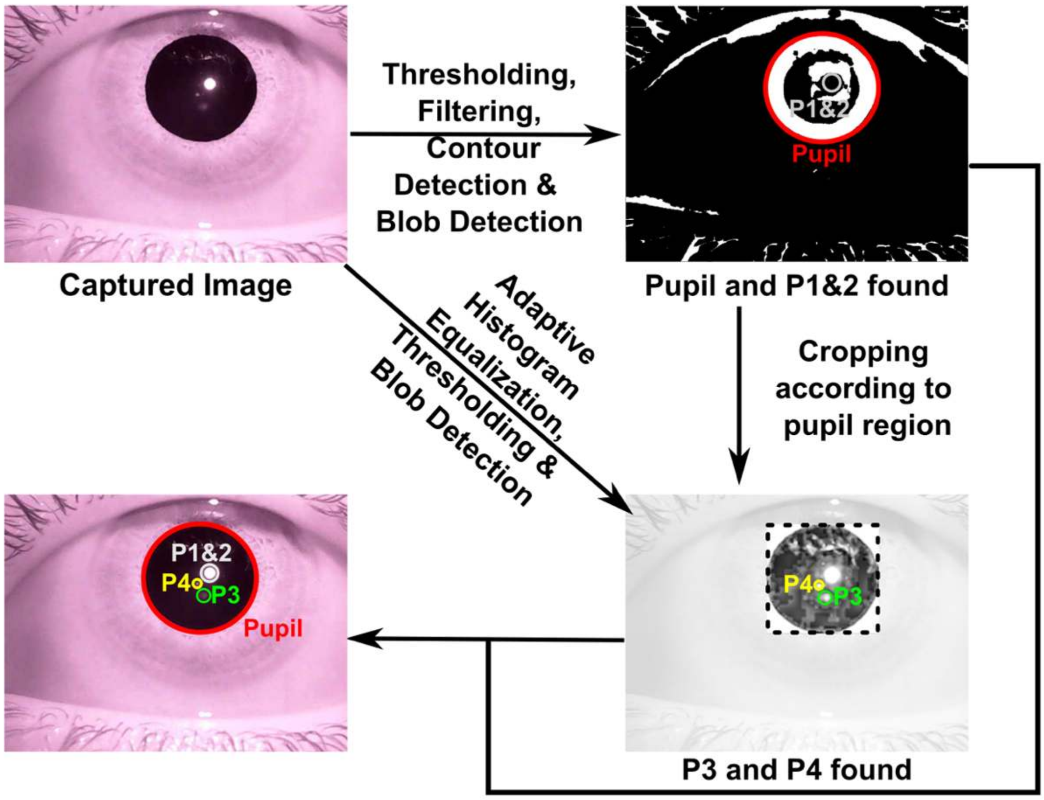

Figure 2.5: Diagram of our image processing algorithm used for finding the Purkinje reflection locations and pupil parameters.

The image processing algorithm led us to identify 10 different parameters. Notably, the abbreviations representing the locations of P1 and P2 will be changed from P1&2 to P1 for simplicity in the remainder of this thesis. Eight of these parameters represent the locations of Purkinje reflections and pupil center (x_{P1}, y_{P1}, x_{P3}, y_{P3}, x_{P4}, y_{P4}, x_{PC} and y_{PC}) in the x (horizontal) and y (vertical) directions in pixels. The other two parameters indicate the pupil size. It may first be unclear why two parameters are used to describe the pupil size, but this is due to the use of elliptical images of the pupil in our off-axis imaging method. These two parameters (r_1 and r_2) correspond to semimajor and semiminor lengths of the ellipse fitted around the pupil. In conclusion, 10 parameters were determined for each frame with the corresponding accommodation distance and vergence angle. The average processing time was calculated as 15 ms for each frame. A zoomed-in version of the camera image showing all 10 parameters is presented in Figure 2.6.

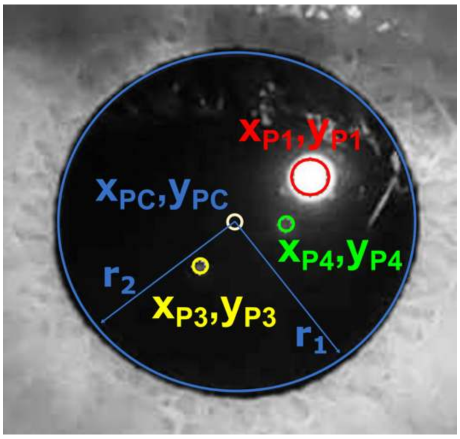

Figure 2.6: A zoomed-in version of camera image that displays all 10 parameters.

Correlation Analyses

We explored the possibility of finding an analytical model relating accommodation/vergence to the locations of Purkinje images by extracting some features from them. Some of these features can be listed as the vertical, horizontal, and Euclidean distances between P1 and P3 or P4, as well as the angles between P1, P3, or P4. It has been observed that certain features correlate with accommodation, while others exhibit a relationship with vergence. Therefore, we carried out individual correlation analyses for each subject between the extracted features and the accommodation of corresponding target points in CF1 to determine the parameters most related to accommodation. Similarly, correlation analysis was performed between the extracted features and the vergence of corresponding target points in CF2. As a result, we obtained the Pearson correlation coefficient, which is an indicator of the linear correlation between two sets of variables, in our case for various features and accommodation or vergence. This enabled us to explore the possibility of establishing a linear relationship between these features and accommodation or vergence for each individual subject. All analyses were performed with a custom-written MATLAB script, and the “corr” function from the Statistics and Machine Learning Toolbox (Math Works) was used.

First ML Approach: Subject-Specific Analysis

After exploring the relationship between some features extracted from the Purkinje reflection locations and accommodation/vergence, I explain our initial ML approach in this subsection. In this approach, we treated the data from each subject as separate datasets and evaluated our model individually for each. Therefore, this approach primarily enabled us to evaluate the performance of our ML model in predicting accommodation/vergence using the data from each subject separately. I will explain our leave-one-subject-out cross-validation (LOSO-CV) approach, which is suitable for a wider range of applications, in the following subsection.

Different types of ML models exist for predicting continuous variables, such as decision tree regression, support vector machines, multilayer perceptron (MLP) and random models. First, we investigated these different ML approaches. Among these approaches, the MLP was chosen due to its ability to handle high-dimensional data and model complex nonlinear relationships.

After selecting the algorithm, the input and output parameters were determined. In our initial approach, two different combinations of input parameters were determined, which enabled us to determine the effects of the parameters on the outputs. These two combinations can be listed as follows: only the locations of Purkinje images (x_{P1}, y_{P1}, x_{P3}, y_{P3}, x_{P4}, y_{P4}); and the locations of Purkinje images, the pupil center and the pupil size parameters (x_{P1}, y_{P1}, x_{P3}, y_{P3}, x_{P4}, y_{P4}, x_{PC}, y_{PC}, r_1 and r_2). Both parameter groups were given as inputs to the model. Furthermore, our model was designed to provide two outputs at the same time: the accommodation distance in Diopters and the vergence angle in degrees.

Our next step was to determine the procedure to be followed for splitting the data into training and testing sets. We split the data differently from the standard practices, which generally use 70-80% of the data for training and 30-20% for testing. Since we have approximately 50 to 80 frames for each target point, using a smaller portion of the data from each target point was sufficient to estimate the output values for all other frames. To check for overfitting and model robustness, we also included the training dataset in the testing dataset. Overall, we used 30% of the randomly selected data as the training set and the whole dataset as the testing set. Nine datasets for 9 subjects were trained and tested after splitting the data using this method. Our detailed model structure for subject-specific analysis and evaluation methodology with data splitting is illustrated in Figure 2.7.

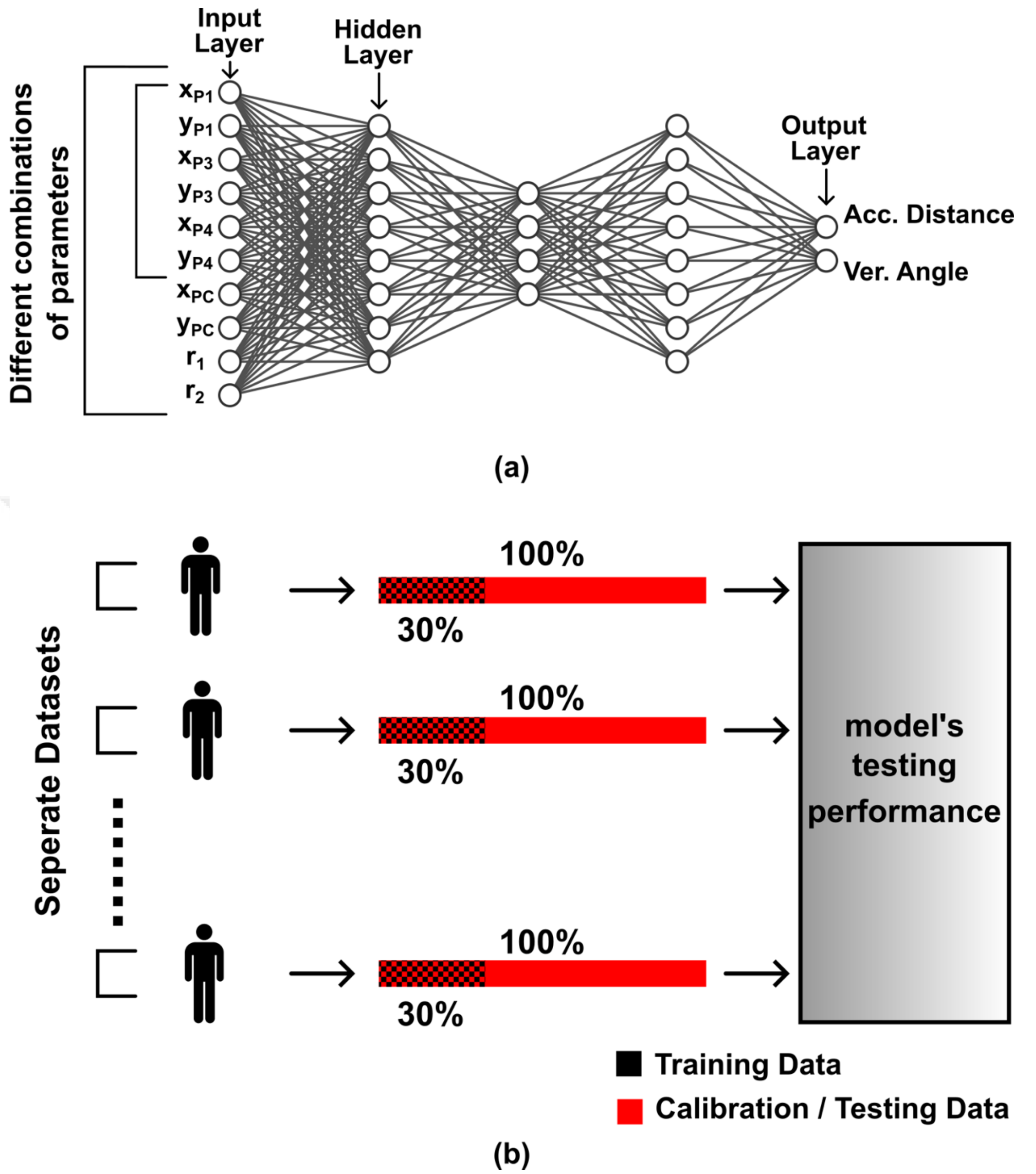

Figure 2.7: Overview of our first approach: subject-specific analysis: (a) our MLP architecture detailing input, hidden, and output layers with varied parameters, (b) data splitting for model testing, showcasing a 30% training and 100% calibration/testing split across separate datasets.

Now that our data splitting procedure has been explained, our MLP model can be described in more detail. Our MLP model consisted of input and output layers and subsequent layers between them, which are all fully connected to the previous and next layers. Except for the output layer, all layers were followed by the ReLU activation function, which helped our model learn nonlinear relationships between the input and output variables. The output layer did not have any activation function since the output variables can be any value and no restrictions should be applied to them. In each iteration, these output variables were found after the input variables passed through the layers, and model accuracy was evaluated by the mean square error (MSE) loss function. This loss function was calculated by taking the average of squares of differences between the true values and predicted values of the output variables. Our model was then optimized by the Adam optimization algorithm according to the MSE loss function.

We explained the MLP model structure that was determined before performing any estimation or prediction. The other parameters, such as the number of dense layers and the number of neurons each contains, batch size, and epoch size, were identified as hyperparameters. Their exact values were determined by hyperparameter tuning for each of the 2 input options and nine datasets. Hyperparameter tuning was applied by a grid search that consisted of specifying candidate values for each hyperparameter and trying all possible combinations to determine the one resulting in the lowest prediction error. After noting the errors from all 9 datasets, the average was calculated to determine the optimal hyperparameter set.

Second ML Approach: Leave-One-Subject-Out Cross-Validation Analysis

Noting that in the subject-specific analysis, we did not consider the similarities between multiple images from the same target point and subject while splitting the data, our results may be significantly affected if tested again with different subjects. Therefore, we proposed a leave-one-subject-out cross-validation (LOSO-CV)-based analysis and prediction scheme to develop an estimation method that is more robust to subject variations. In this approach, the multilayer perceptron (MLP) technique was employed again, and the model structure was adopted, with the exception of the dataset, splitting procedure and number of models for each output.

First, differing from the subject-specific analysis, we treated the data collected from all subjects as one large dataset in the LOSO-CV-based analysis. Second, these data were split into training, calibration and testing sets based on the subjects in accordance with the working principle of the LOSO-CV method. Rather than evaluating the individual datasets only once, as in the subject-specific analysis, LOSO-CV analysis evaluated the same dataset a number of times equal to the number of subjects, while the split differed according to the subjects in each evaluation. For each split, the data from one subject were used for calibration and testing, while the data from all other subjects were used to train the model. The performance of the model was evaluated for each split separately. In our case, the dataset we collected from the left eyes of 9 subjects was split into training, calibration and testing sets in 9 different ways.

The term "calibration set" may initially appear confusing. This term refers to the data used for calibrating the predictions from the testing set through linear transformation. This transformation is applied according to the predictions from the calibration set itself. Specifically, the calibration set corresponds to the data taken from the test subject when they were focusing on the target points at 3.5 D and 1.5 D in each configuration. These target points were named CP1CF1 and CP2CF1 for the first configuration and CP1CF2 and CP2CF2 for the second configuration. The selection of these two target points was based on their ability to cater to a wide variety of visual conditions, including both myopia and hypermetropia. The averages of the predictions from the data for the ith calibration point in the jth configuration were calculated for both accommodation and vergence and were named A_{CPiCFj} and V_{CPiCFj}, respectively. In addition, the uncalibrated prediction results were labeled A_{raw} and V_{raw}, while after calibration, they were named A_{calib} and V_{calib} for the corresponding data point.

Based on these findings, calibration was made for the data points in the second configuration using the following equations:

$$\frac{3.5 - A_{calib}}{A_{CP1CF2} - A_{raw}} = \frac{A_{calib} - 1.5}{A_{raw} - A_{CP2CF2}} \tag{2.2}$$

$$\frac{6.24 - V_{calib}}{V_{CP1CF2} - V_{raw}} = \frac{V_{calib} - 2.68}{V_{raw} - V_{CP2CF2}} \tag{2.3}$$

In these equations, the numerical values correspond to the accommodation distances and vergence angles for the designated target points in the second configuration. The same calculations can also be adapted for the first configuration. Our MLP model structure, which is used for LOSO-CV-based analysis, and our evaluation methodology, which involves data splitting, are illustrated in Figure 2.8a and Figure 2.8b, respectively.

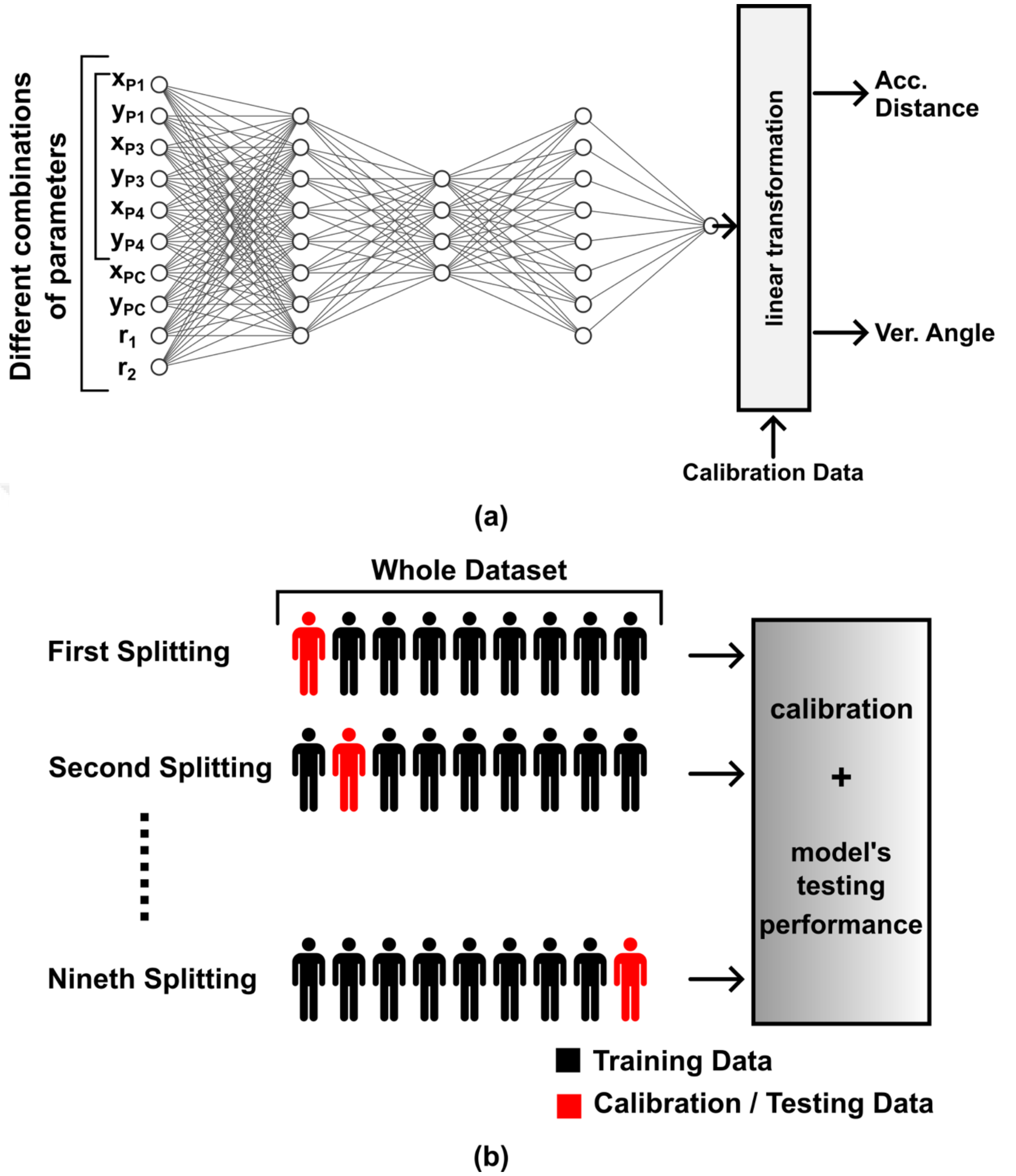

Figure 2.8: (a) Our MLP architecture showcasing input, hidden, and output layers with various parameters, (b) an illustration of data partitioning for model evaluation, demonstrating a leave-one-subject-out cross-validation approach with separate datasets.

To assess the impact of Purkinje reflection positions on measuring accommodation and vergence, we employed the feature importance technique during the leave-one-subject-out cross-validation (LOSO-CV) approach. This method involves randomly shuffling the values of a specific feature in the dataset and then using the algorithm to generate estimates from this modified dataset. The subsequent performance decline of the model highlights the significance of the feature in predictions. We applied this technique separately to CF1 and CF2 to discern key features in configurations primarily altering vergence and accommodation.

2.3 Results

In this section, we present the simulation results performed to understand the formation of the reflections, along with the accommodation and vergence measurement results from various estimation methods across nine subjects.

2.3.1 Simulation Results

The simulation results performed to understand the formation of Purkinje reflections are provided in this subsection. These results were compared with the experimental data for some subjects. They matched for certain configurations, especially for the CF2, where vergence was present. Figure 2.9 demonstrates this match by displaying the images captured by the camera and screenshots from the ZEMAX detector viewer, corresponding to accommodation depths of 4 D, 2.5 D, and 1 D for CF2, respectively. Additionally, by looping through various combinations within a range of positions for the components, we were able to determine whether the relative positions of the camera LED and eye at the extremes of configuration extremes cause any reflection to not be visible or overlap with each other.

2.3.2 Accommodation and Vergence Prediction based on Features Determined by Correlation Analysis

The results of the correlation analysis between the features extracted from the Purkinje reflections and accommodation/vergence revealed that some features were highly correlated with accommodation, while others were highly correlated with vergence. By “highly correlated”, we mean that the Pearson correlation coefficient is between 1 and 0.8. Among these highly correlated features, the vertical distance between P3 and P4 ($v_{P3,P4}$) in pixels (px) was the most strongly correlated feature with accommodation, and the Euclidean distance between P1 and P4 ($d_{P1,P4}$) in px was the most strongly correlated feature with vergence, reaching the maximum ρ values.

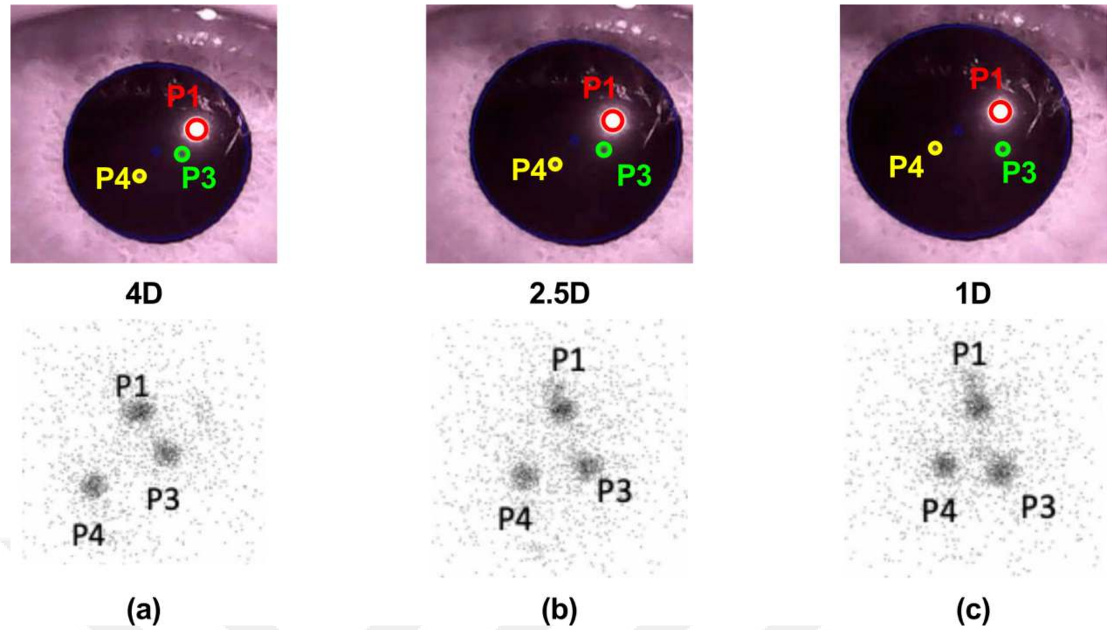

Figure 2.9: Alignment of experimental results with simulations across varying accommodation depths. Images of the eye at the top row showing locations of Purkinje reflections at varying accommodation depths. ZEMAX detector viewer screenshots at the bottom row displaying the simulated distribution of Purkinje images. (a), (b) and (c) represent 4, 2.5 and 1 D, respectively.

To observe the relationship between these features and accommodation/vergence for each subject individually, we calculated $v_{P3,P4}$ and $d_{P1,P4}$ for each frame and noted the target accommodation and vergence from the corresponding target point. Assuming that the target accommodation can be expressed as a linear function of $v_{P3,P4}$ and that the target vergence can be expressed as a linear function of $d_{P1,P4}$, we applied linear regression to identify the linear relationships between features and target values. Figure 2.10 illustrates the linear regression analysis conducted to express the relationship between accommodation and $v_{P3,P4}$ (on the left) and the relationship between accommodation and $d_{P1,P4}$ (on the right) for subjects #4 and #9. The x-axes represent features measured in px, while the y-axis represents the accommodation distance in D or the vergence angle in degrees. A boxplot is provided to illustrate the distribution of the features for each accommodation distance or vergence distance. In the accommodation case, the solid line represents the best fitted line with the slope of a_{acc} in D/px and the x-intercept of b_{acc} in px. In the vergence case, the solid line represents the best fitted line with the slope of a_{ver} in deg/px and the x-intercept of b_{ver} in px.

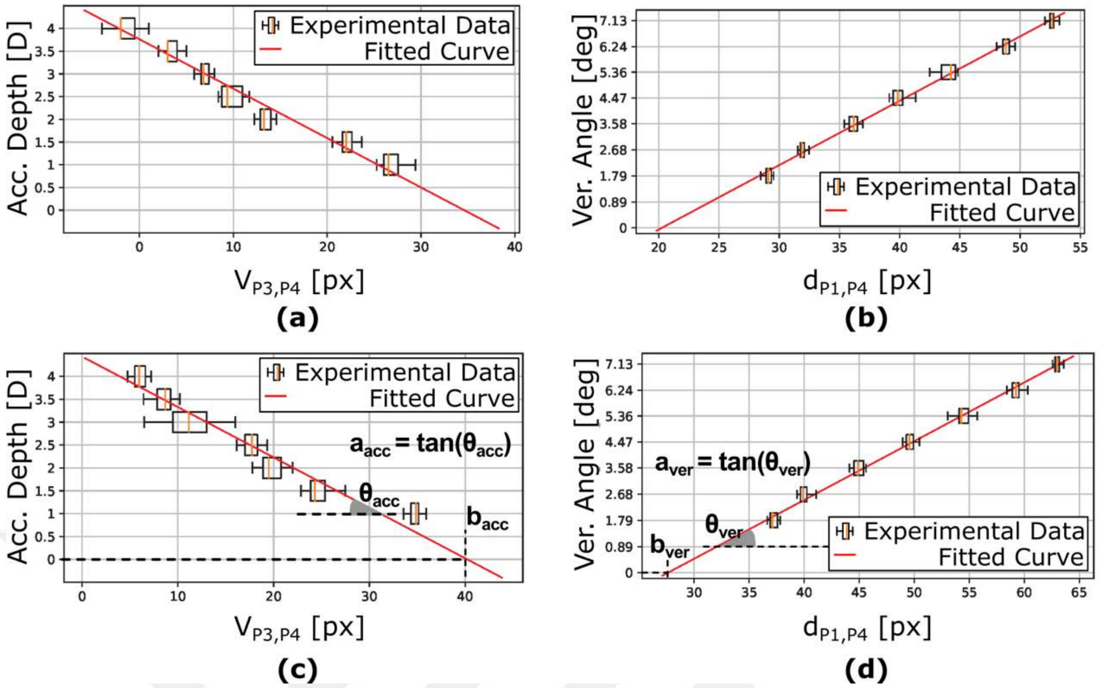

Figure 2.10: Linear regression analysis conducted to express the relationship between accommodation and $v_{P3,P4}$ (on the left) and the relationship between accommodation and $d_{P1,P4}$ (on the right) for subjects #4 (top) and #9 (bottom). (a,c) The solid line represents the best fitted line with the slope of a_{acc} in D/px and the x-intercept of b_{acc} in px. (b, d) The solid line represents the best fitted line with the slope of a_{ver} in deg/px and the x-intercept of b_{ver} in px.

The linear relationships modeled through linear regression are expressed mathematically in Equations 2.4 and 2.5:

$$A\,[D] = a_{acc}(v_{P3,P4} - b_{acc}), \quad v_{P3,P4} = y_{P4} - y_{P3} \tag{2.4}$$

$$V[deg] = a_{acc}(d_{P1,P4} - b_{ver}), \; d_{P1,P4} = \sqrt{(y_{P4} - y_{P3})^2 + (x_{P4} - x_{P3})^2} \tag{2.5}$$

Using all samples of each individual dataset allows us to capture all available trends and patterns within the data. After finding a linear relationship by using regression methods, the same model can be reapplied individually to the datasets to check the accuracy of the model by comparing the predicted values and the target accommodation values. In addition, this allows us to observe the fluctuations within the dataset that our linear model could not handle. We reapplied the linear models we obtained to the data to determine the model accuracy and observe the fluctuations within the same target point over time. In Figure 2.11, the predicted values of accommodation and vergence over time are illustrated for subjects #4 and #9.

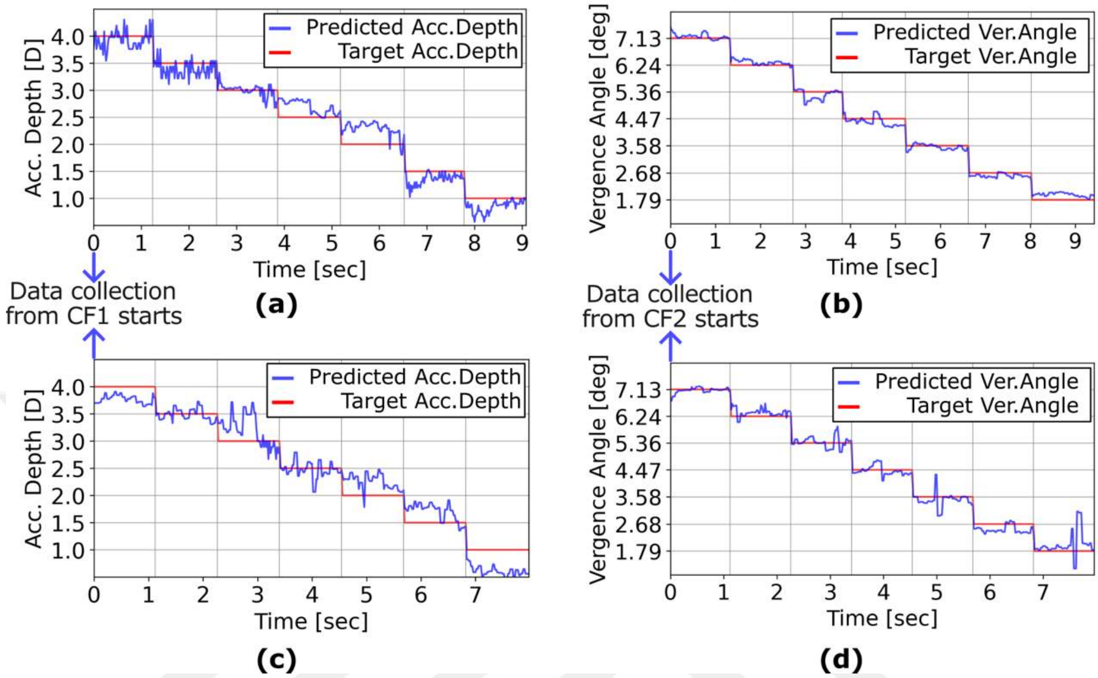

Figure 2.11: Predicted accommodation and vergence derived from features determined by correlation analysis over time for subjects #4 and #9. Subfigure (a) shows the accommodation predictions for Subject #4, subfigure (b) depicts the vergence for Subject #4, subfigure (c) presents the accommodation for Subject #9, and subfigure (d) shows the vergence for Subject #9.

In addition to the results per data point, we also calculated averages across each target accommodation depth and vergence angle. This enabled us to determine whether our analysis can be used for finding accommodation and vergence under conditions where subjects fixate on a specific point for a defined duration. The mean values of the predicted accommodation distances and vergence angles at all target accommodation and vergence angle levels for all 9 subjects are shown in Figure 2.12. Each color in the figure corresponds to one subject, and the dashed line corresponds to the point where the target and predicted values are equal.

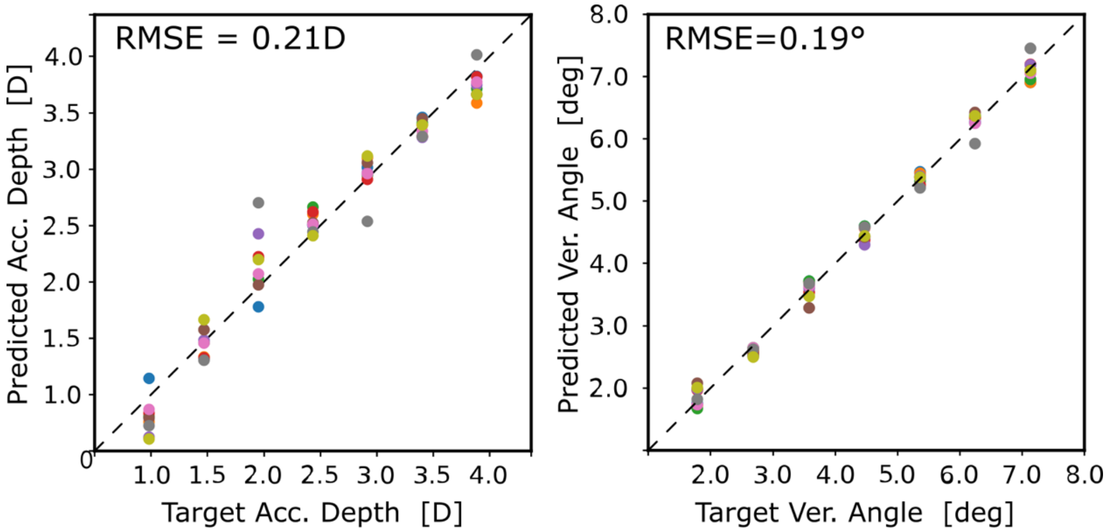

(a) **(b)**

Figure 2.12: Mean values of accommodation distance and vergence angle derived from features determined by correlation analysis. (a) Target accommodation depth versus predicted accommodation depth, calculated across the data points corresponding to each target point in CF1, for all 9 subjects. (b) Target vergence angle versus predicted vergence angle, calculated across datapoints corresponding to each target point in CF2, for all 9 subjects.

The analyses were repeated for all subjects, and model accuracy was obtained by comparing the predicted and target accommodation values. This was achieved by calculating the root mean square error (RMSE), which is a measure of residuals, and the coefficient of determination (R^2), which is a measure of correlation. These calculations were performed separately for each data point using a single-frame analysis and for the averages computed across each target accommodation distance and vergence angle, a process referred to as ensemble averaging. These metrics were denoted as A_{RMSE}, $A_R{}^2$, $A_{RMSE(avg)}$, and $A_R{}^2{}_{(avg)}$ for accommodation and V_{RMSE}, $V_R{}^2$, $V_{RMSE(avg)}$, and $V_R{}^2{}_{(avg)}$ for vergence, respectively. The resulting accuracy metrics for each subject are provided in Figure 2.13. As can be interpreted from the figure, the ensemble averaging results were better than those of the single-frame analysis for each subject, as expected. On the other hand, vergence can be predicted with an accuracy lower than 0.25 deg.

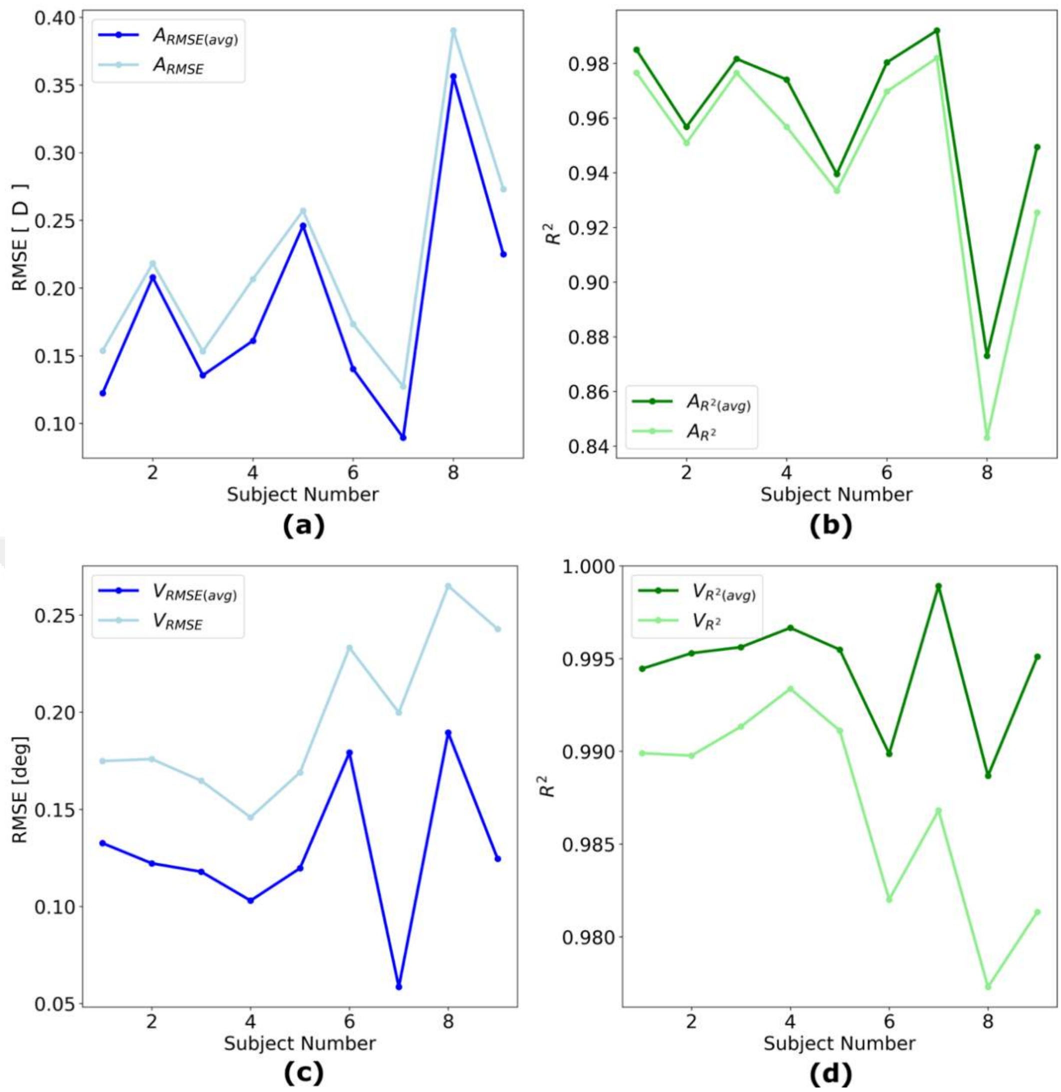

Figure 2.13: Graphs showing the accuracy of our correlation analysis-based method for both accommodation and vergence across all subjects using the root mean square error (RMSE) and coefficient of determination (R^2). The graphs show both per data point and by ensemble averaging (denoted with avg) results for (a) the RMSE for accommodation, (b) the R^2 for accommodation, (c) the RMSE for vergence, and (d) the R^2 for vergence.

2.3.3 Accommodation and Vergence Prediction from Subject-Specific MLP Analysis

The results from the subject-specific MLP analysis are provided in this subsection. Before we begin, unlike in the correlation analysis, data from both CF1 and CF2 were combined and used for the training and testing of the results.

As a first step, hyperparameter tuning was performed, and the values of the hyperparameters that resulted in the highest accuracies were listed. A batch size of 20 and 300 epochs resulted in the highest average accuracy for both combinations of input parameters, as mentioned in the Methods section.

The results for each subject were subsequently obtained separately. Figure 2.14 and Figure 2.15 illustrate the predicted values of accommodation and vergence for every frame in the testing dataset of subject #9 (meaning that all data for that subject) over time. Figure 2.14 presents the results from the first set of input parameters, and Figure 2.15 from the second set, which includes pupil parameters.

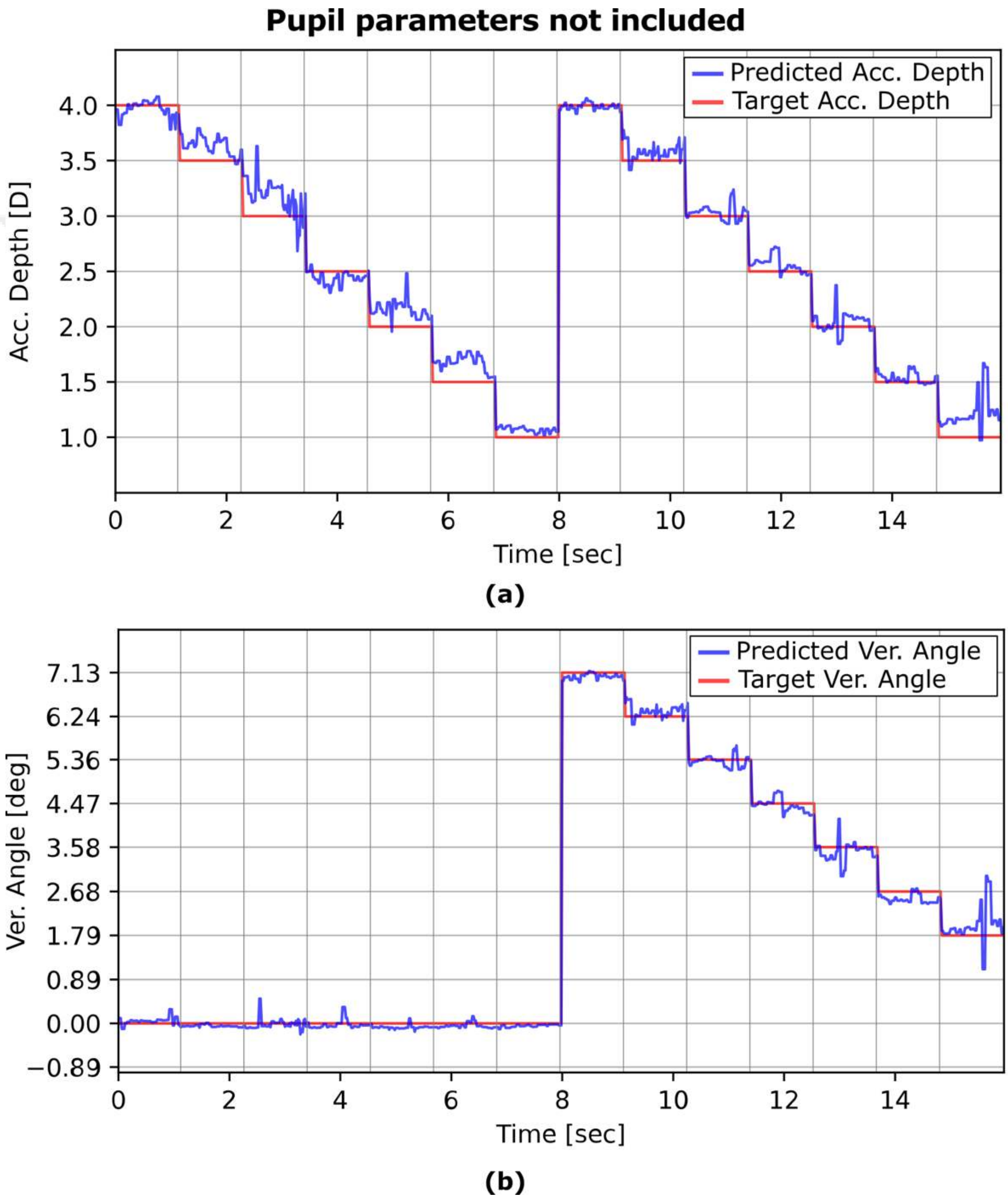

Figure 2.14: Predicted values of (a) accommodation distance and (b) vergence angle for each frame in the testing dataset of Subject #9 over time, derived from subject-specific analysis using the first set of input parameters.

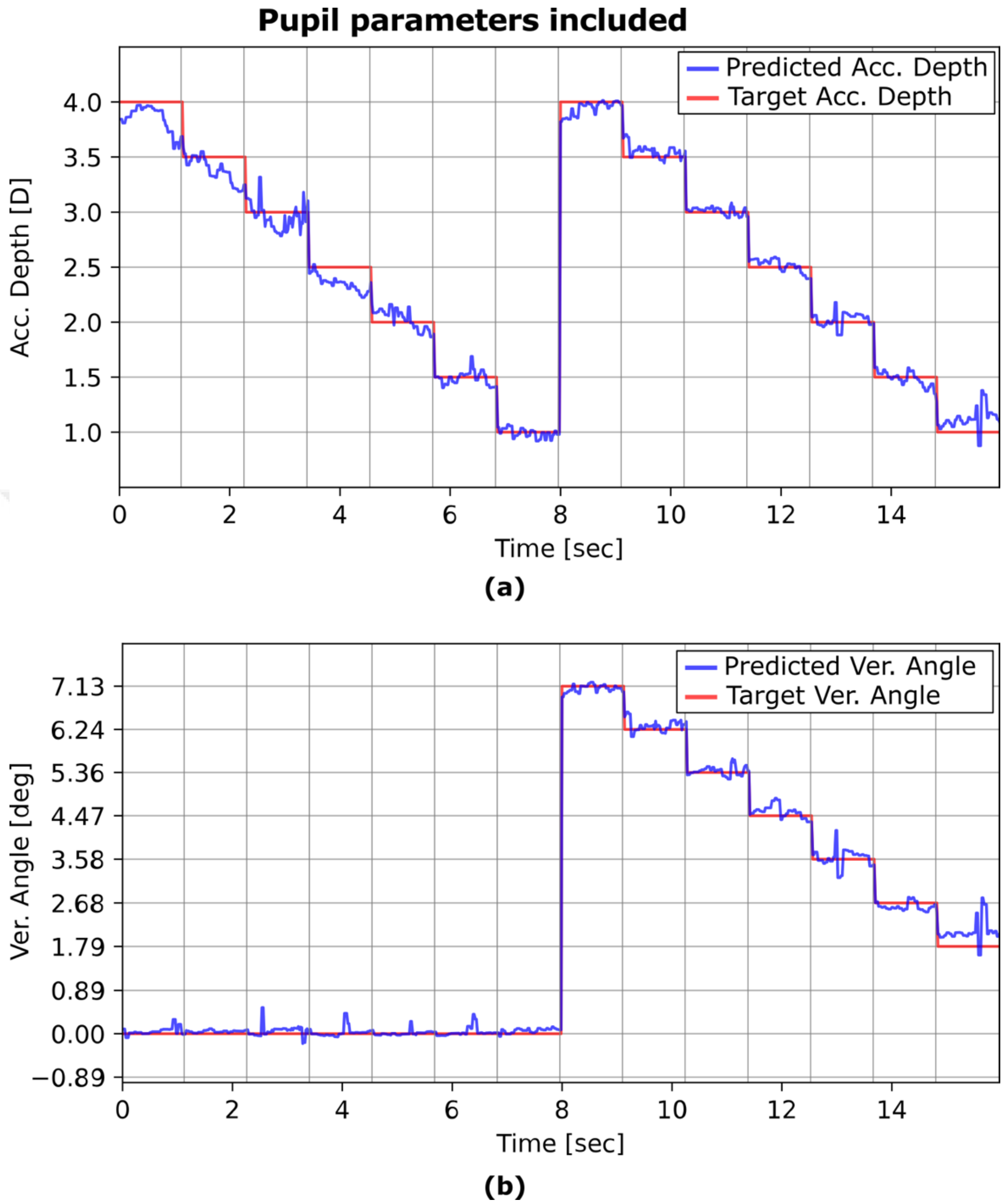

Figure 2.15: Predicted values of (a) accommodation distance and (b) vergence angle for each frame in the testing dataset of Subject #9 over time, derived from subject-specific analysis using the second set of input parameters.

The results suggest that the pupil parameters have a small impact on the prediction, while they result in good average values for some of the target points, which worsened the results for the others for subject #9. To further analyze the impact of the pupil parameters in the second set of input parameters, we visualized the change in pupil size with increasing accommodation for CF2 from subject #5 in Figure 2.16a. In addition, the evaluation metric A_{RMSE} was calculated for both cases via a similar procedure that was followed by correlation analysis, and the resulting A_{RMSE} for each subject is provided in Figure 2.16b. The A_{RMSE} was chosen for the comparison between two sets of input parameters since it is a measure of deviation for our main metric of interest, accommodation.

Figure 2.16a indicates that the pupil size decreases with increasing accommodation, as expected. However, fluctuations in pupil size are observed that could be due to factors such as varying illumination conditions. On the other hand, the analysis of the influence of pupil size on model accuracy showed that pupil size parameters do not significantly enhance the prediction accuracy of the model. Specifically, the $A_{RMSE(avg)}$ shows variations among subjects: it increases slightly for some subjects and decreases for others.

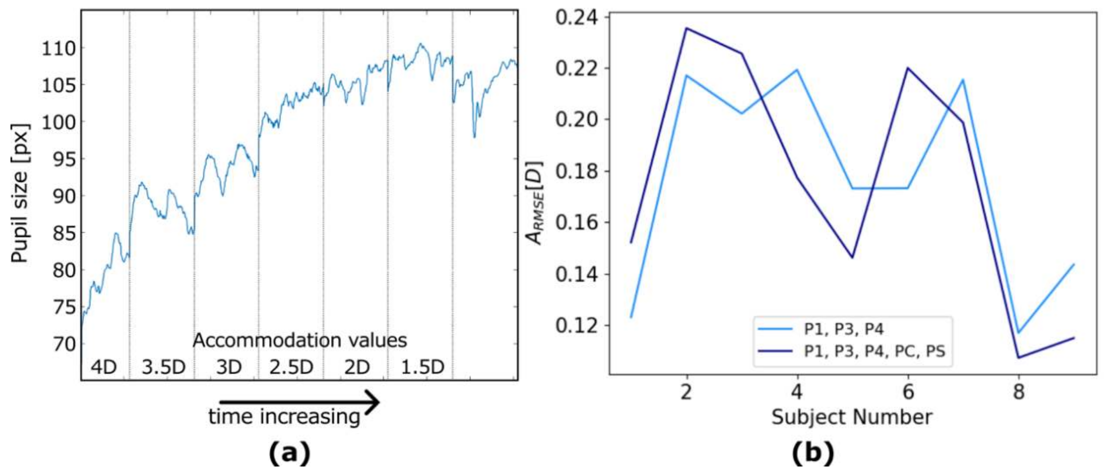

Figure 2.16: (a) The relationship between accommodation and pupil size based on data obtained from CF2 for Subject #5. (b) $A_{RMSE(avg)}$ metrics derived from subject-specific analysis using two distinct sets of input parameters.

Finally, we calculated averages for each target accommodation depth and vergence angle using only the first set of input parameters, as pupil parameters did not improve the results. This allowed us to evaluate whether our subject-specific analysis could determine accommodation/vergence when subjects fixated on a point for a predefined duration. The mean predicted values versus the target levels for all 9 subjects are shown in Figure 2.17.

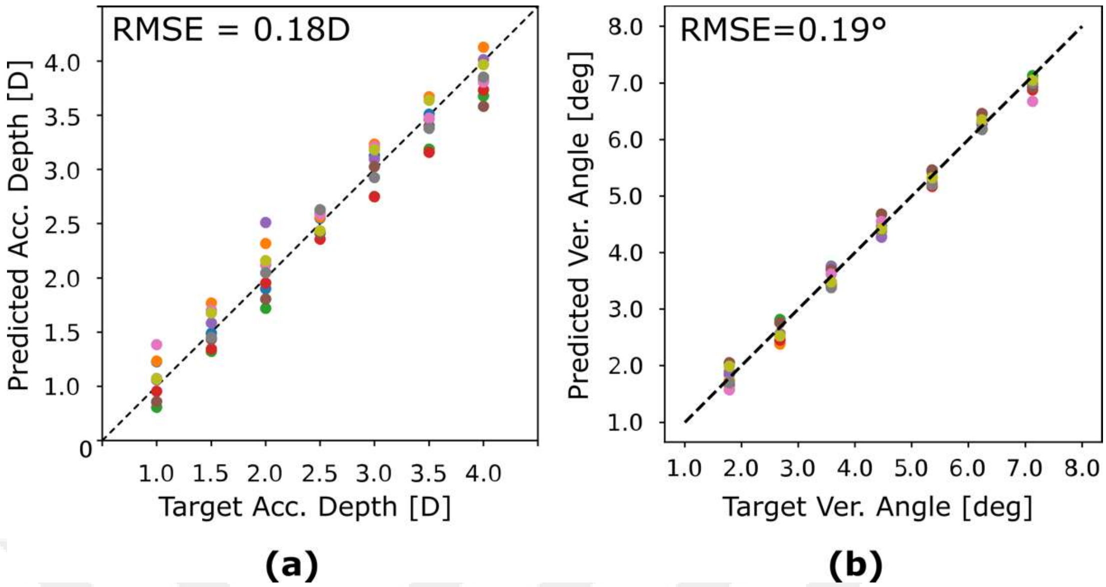

Figure 2.17: Mean values of accommodation distance and vergence angle derived from our subject-specific analysis scheme. (a) Target accommodation depth versus predicted accommodation depth, calculated across the testing dataset for all 9 subjects separately. (b) Target vergence angle versus predicted vergence angle, calculated across the testing dataset for all 9 subjects.

Effect of Interocular Variability on the Results

This subsection presents subject-specific results from the right eye of subject #5, organized from 4 D to 1 D, to assess interocular variability. To make a comprehensive comparison, the results were provided for both the left and right eyes of subject #5 using two distinct sets of input parameters. Figure 2.18 the results obtained using the first set of input parameters for both the left and right eyes of the subject, allowing us to directly compare the outcomes side by side. Figure 2.19 illustrates the results using the second set of input parameters, following the same methodology.

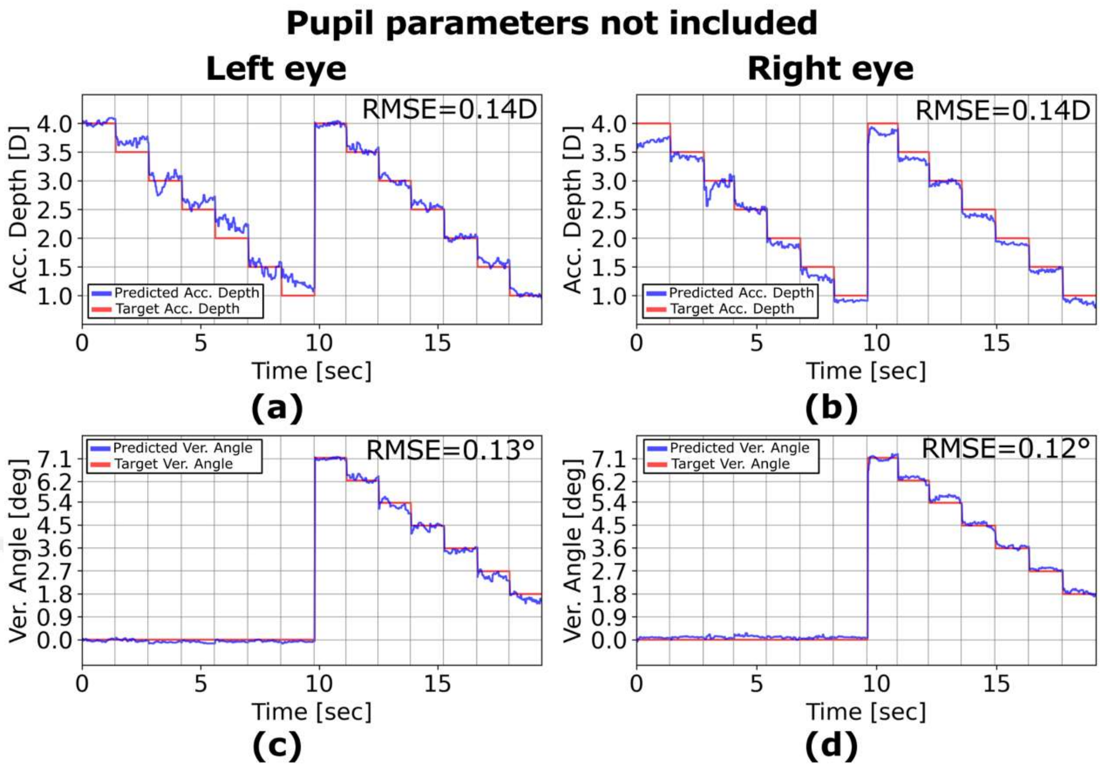

Figure 2.18: The subject-specific analysis results obtained using the first set of input parameters for both the (a,c) left and (b,d) right eyes of subject #5.

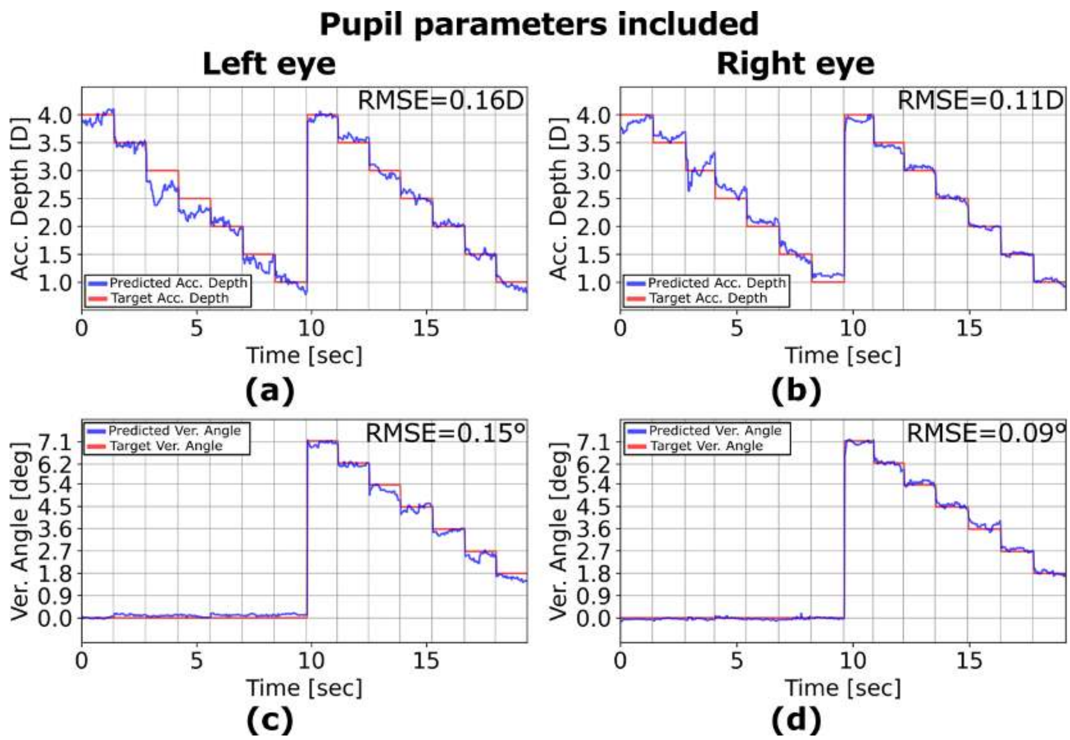

Figure 2.19: The subject-specific analysis results obtained using the second set of input parameters for both the (a,c) left and (b,d) right eyes of subject #5.

Effect of Data Collection Procedure on Results

The results from a subject-specific analysis of data from the left eye of subject #5 in the randomized procedure, where LEDs were turned on and off in a random sequence to mitigate the effects of habituation, are provided in this section. The results only show the results from the randomized procedure since the results from the normal data procedure (from 4 D to 1 D in descending order) from subject #5 were already presented in the previous subsection. Figure 2.20 presents the results of the subject-specific analyses, which were derived from data collected through both standard and randomized procedures using both sets of input parameters. The results revealed that there were fluctuations around the target accommodation distance or vergence angle in the case of the randomized procedure. These fluctuations increase even more when the pupil parameters are included as input variables.

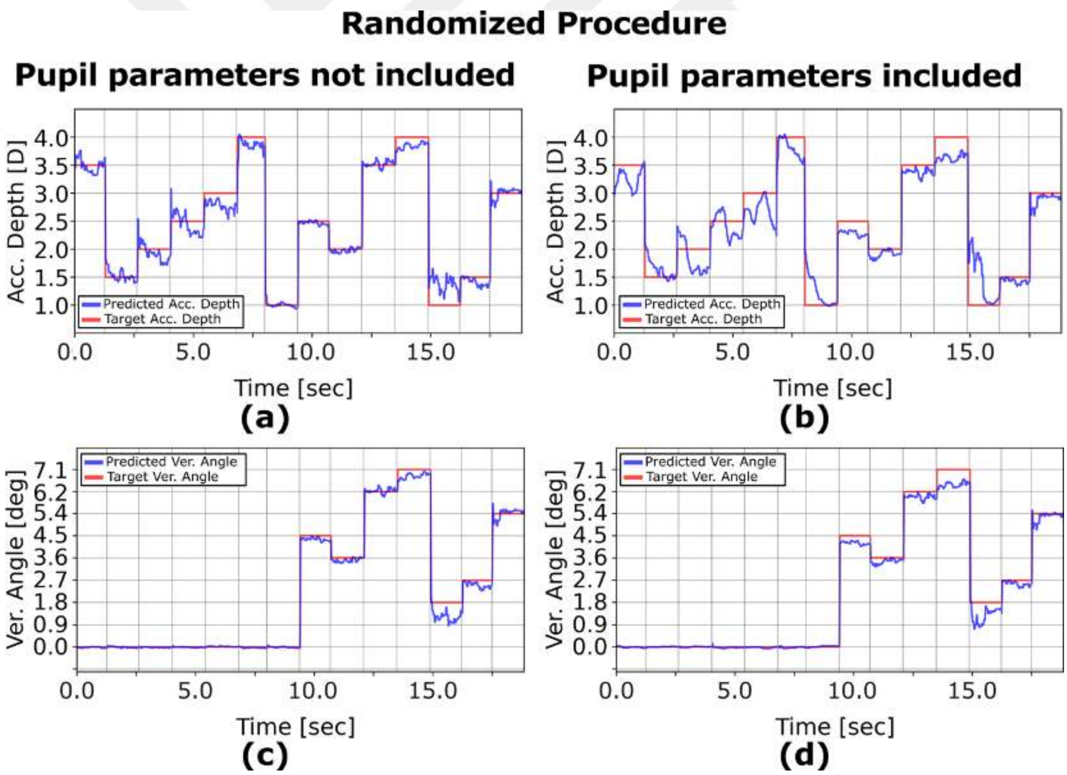

Figure 2.20: The subject-specific analysis results from data from the left eye of subject #5 in the randomized procedure.

Assessing Repeatability of Measurements

The repeatability of the measurements was tested by repeating the data collection procedure and analysis for two subjects and calculating the Pearson correlation coefficient (r) and p-value, as mentioned in the Methods section. The results from our subject-specific approach using the first set of input parameters showed that the measurements from the same subject were highly correlated (r = 0.99, p < 0.001 for both subjects).

2.3.4 Accommodation and Vergence Prediction from Leave-One-Subject-Out Cross-Validation Analysis

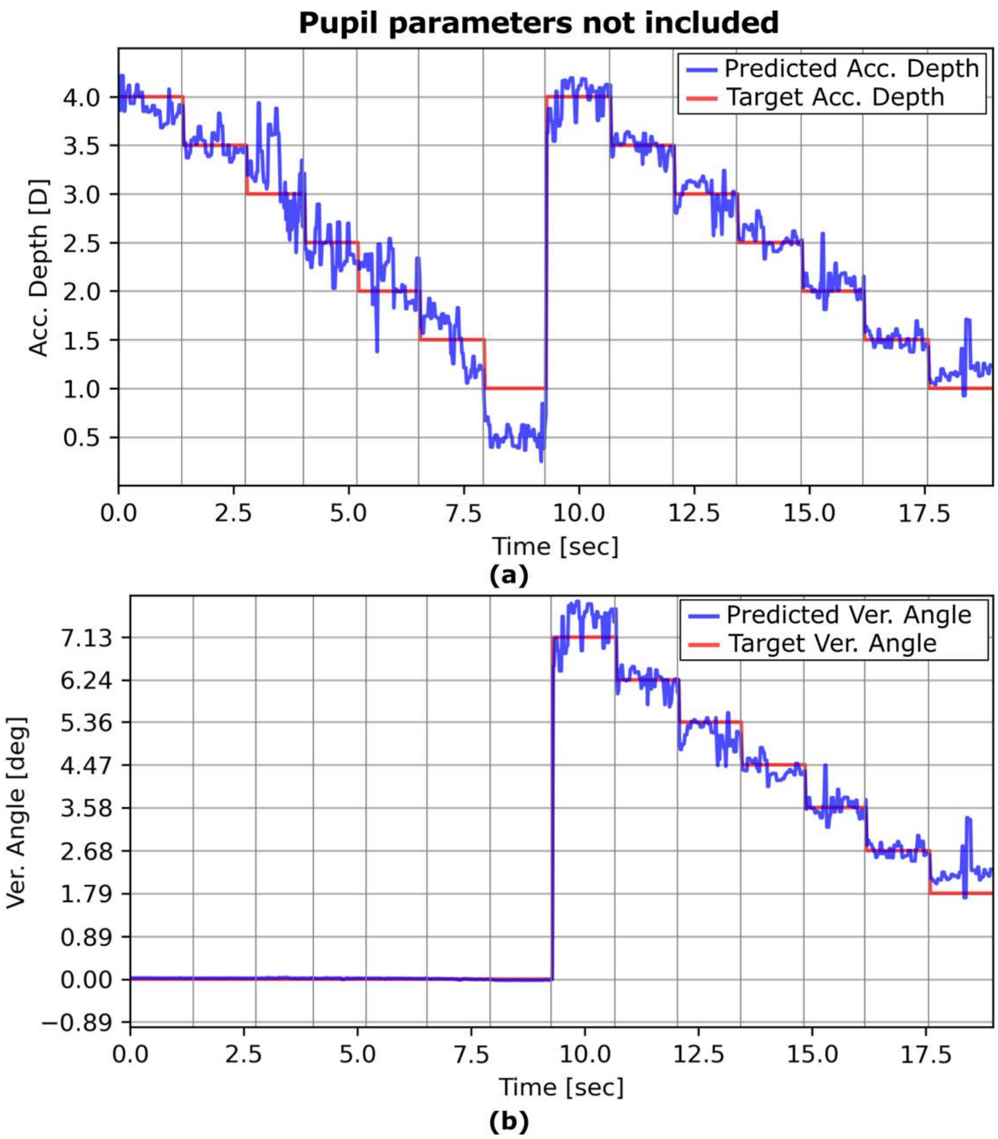

Figure 2.21: Predicted values of (a) accommodation distance and (b) vergence angle for each frame in the testing dataset of Subject #7 over time, derived from LOSO-CV analysis using the first set of input parameters.

The results from the MLP analysis using the LOSO-CV method are provided in this subsection. As a first step, hyperparameter tuning was performed, and the values of the hyperparameters that resulted in the highest accuracies were listed. A batch size of 40 and number of epochs of 400 resulted in the highest average accuracy for both combinations of input parameters, as mentioned in the Methods section.

Subsequently, the results for each subject were obtained separately. Figure 2.21 and Figure 2.22 graphically depict the predicted values of accommodation and vergence over time for each frame in the dataset of subject #7. These predictions are performed by the MLP trained on a dataset that includes all the data except for the subject's own data. Figure 2.21 displays the results obtained from the MLP model using the first set of input parameters, while Figure 2.22 shows the results from the second set, which includes the pupil parameters.

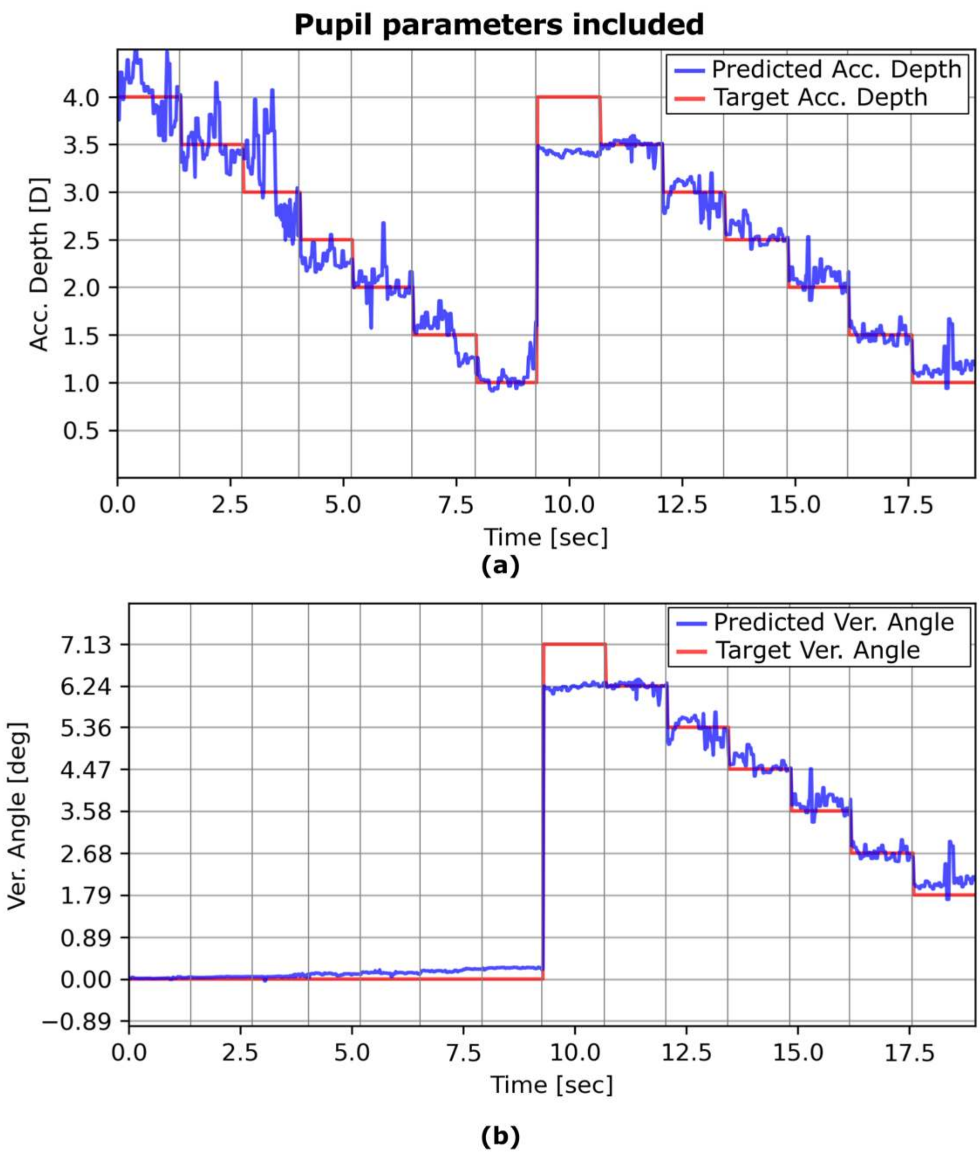

Figure 2.22: Predicted values of (a) accommodation distance and (b) vergence angle for each frame in the testing dataset of Subject #7 over time, derived from LOSO-CV analysis using the second set of input parameters.

The results suggest that the pupil parameters have a significant impact on the prediction, which generally worsened the results for subject #7. To further analyze the impact of the pupil parameters in the second set of input parameters, we calculated and visualized the evaluation metrics A_{RMSE} and V_{RMSE} for both cases in a similar procedure that was followed by the other analyses, and the resulting metrics for each subject are provided in Figure 2.23. The A_{RMSE} and V_{RMSE} were chosen for the comparison between two sets of input parameters since they are measures of deviation.

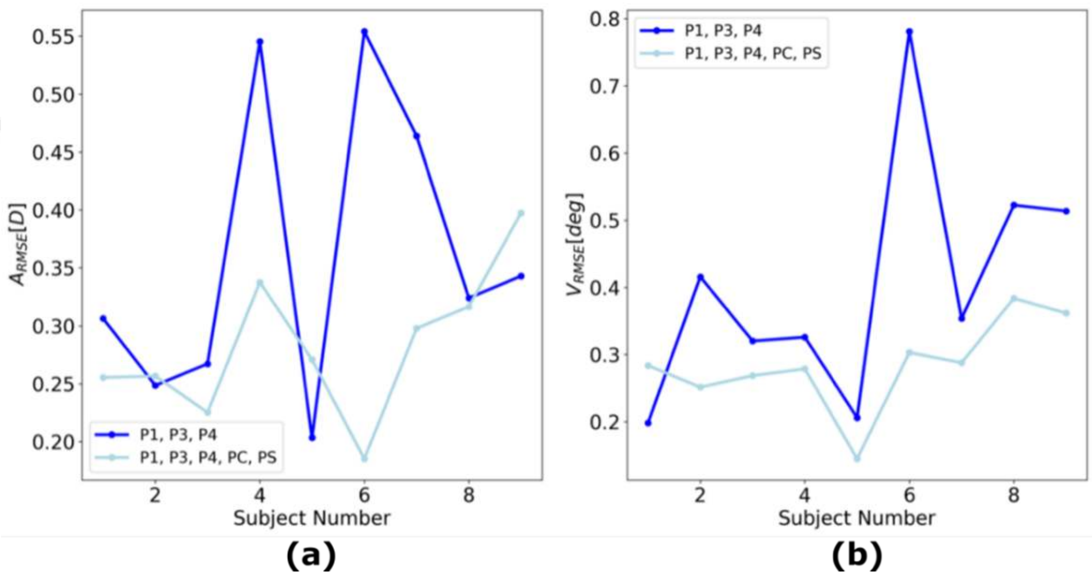

Figure 2.23: RMSE performance of the LOSO-CV method in predicting accommodation and vergence using two distinct sets of input parameters, across all subjects: (a) RMSE for accommodation; (b) RMSE for vergence.

As shown in Figure 2.23, adding pupil parameters significantly worsened the results. Therefore, we used the first set of input parameters to calculate averages for each target accommodation depth and vergence angle. We then tested if our subject-specific analysis could assess accommodation/vergence during fixation on a specific point for a set duration. The mean predicted values for all 9 subjects are shown in Figure 2.24.

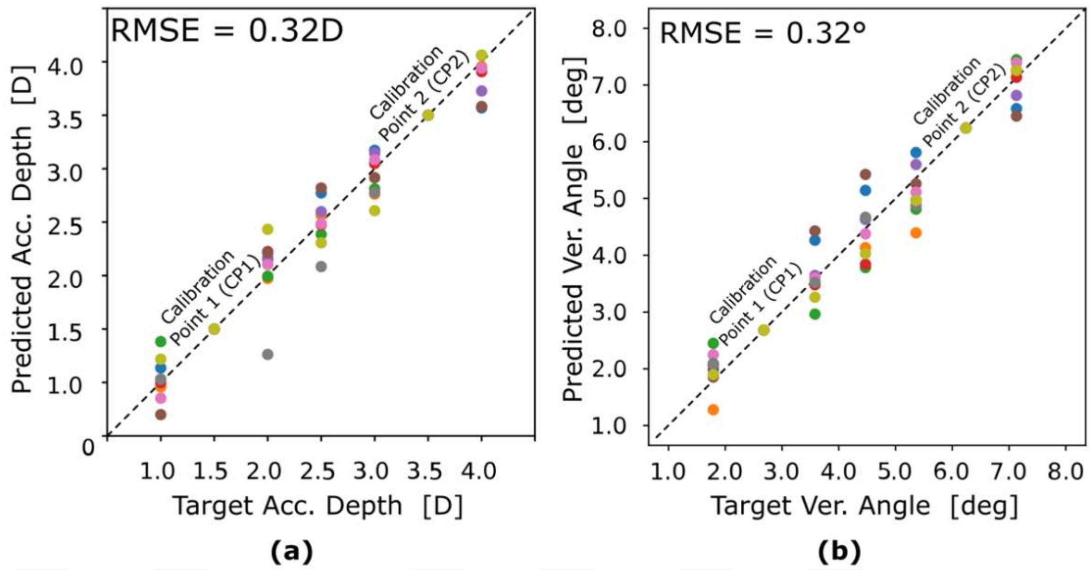

Figure 2.24: Mean values of accommodation distance and vergence angle derived from our LOSO-CV analysis scheme.

Feature Importance

As previously explained, to assess the impact of Purkinje reflection position on measuring accommodation and vergence, we employed the permutation feature importance technique during the leave-one-subject-out cross-validation (LOSO-CV) approach. The feature importance results from the permutation importance technique are shown in Figure 2.25.

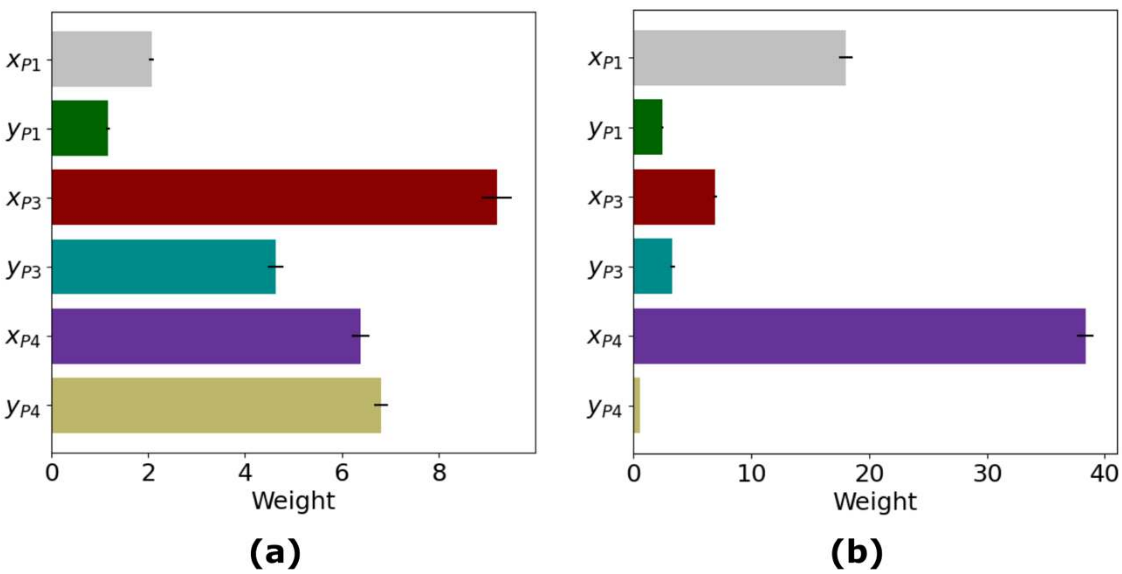

Figure 2.25: Relative importance of Purkinje reflection locations used as inputs in the LOSO-CV-based MLP model for (a) CF1 and (b) CF2.

The relative weights of x_{P1}, y_{P1}, x_{P3}, y_{P3}, x_{P4}, and y_{P4} were 0.23 ± 0.005, 0.13 ± 0.004, 1.0 ± 0.035, 0.50 ± 0.017, 0.69 ± 0.020, and 0.74 ± 0.015, respectively, for CF1. These results revealed that P1 was the least important Purkinje reflection in CF1, where only accommodation changed. On the other hand, the relative weights of x_{P1}, y_{P1}, x_{P3}, y_{P3}, x_{P4}, and y_{P4} were 0.47 ± 0.015, 0.06 ± 0.002, 0.18 ± 0.005, 0.09 ± 0.005, 1.0 ± 0.019, and 0.01 ± 0.001, respectively, for CF2. According to these results, the most important parameter for CF1, where accommodation changes occur, is x_{P3}, and the most important parameter for CF2, where vergence is the dominant change, is x_{P4}.

2.4 *Discussion*

In this work, we proposed three different approaches for identifying accommodation and vergence from Purkinje reflections. The accuracies of the models used in the thesis are presented in Table 2.2.

Table 2.2: Comparison of different methods and different sets of parameters given as inputs to the model

	Depth error [D]	Angle error [deg]
Analytical Function	0.21	0.19
ML trained with own data using P1, P3, P4	0.18	0.16
ML trained with own data using P1, P3, P4, PC, PS	0.17	0.18
ML trained with others' data using P1, P3, P4	0.32	0.32
ML trained with others' data using P1, P3, P4, PC, PS	0.36	0.4

As shown in the table, our subject-specific analysis predicts accommodation and vergence with the best accuracy. However, it utilizes data from all target points, which increases model accuracy. This model does not suggest any improvement by using pupil parameters as input. Our feature-based correlation analysis method achieves good accuracy, demonstrating that the relationship can indeed be established. However, this method employs all the data for analysis. Last, and most importantly, our LOSO-CV results reached an average accuracy of approximately 0.32 dioptres. The significance of this method lies in its ability to predict the accommodation and vergence of a subject by using data from other subjects with only two-point calibration. The accuracy of this method is significantly lower than that of subject-specific analysis, especially for some subjects. This may be because pupil responses during the experiments vary among individuals based on several factors, from lighting conditions to the subject’s emotional states. This suggests that the use of pupil size is not convenient for the LOSO-CV method. The results obtained using the LOSO-CV method fluctuate much more than those of the subject-specific analysis. This could be due to the pronounced effect of fluctuations in the LOSO-CV method.

Regarding the repeatability and reproducibility tests, the results indicate a high correlation between measurements; however, the subjects’ alertness and misplacement of the eye may cause the measurements to deviate from each other. The results from additional tests to observe the effects of interocular variability and randomized procedures revealed that those obtained through subject-specific analysis are not affected by interocular variability. Moreover, including pupil parameters improved the results for the right eye and decreased the performance of the results obtained from the left eye. This can be explained by the fact that the experiments were conducted at different times, and subjects' pupil responses may be influenced by various factors.

One of the most interesting observations was made while observing the effect of the randomized procedure. The results suggest that the subject may experience a lag or lead of accommodation more easily when there are large differences between two consecutive target accommodation distances and vergence angles. Additionally, fluctuations were observable in the results, potentially due to the unpredictability of the next visual stimulus. When the effect of pupil size was also included, the results worsened and became more variable in the randomized procedure.

Chapter 3:
CONCLUSION

In this thesis, we explored the measurement of eye accommodation and vergence using Purkinje reflections and machine learning techniques to develop a novel, more compact, and highly accurate method. This innovative approach has the potential to replace existing biomedical devices, which have limitations because they are bulky and cannot accurately measure eye accommodation dynamically.

This research is based on the utilization of all four Purkinje reflections, which have not been previously explored to this extent in the field of dynamic eye measurements. The use of these reflections with advanced machine learning algorithms, in our case, multilayer perceptron (MLP) networks, resulted in higher levels of prediction accuracy. Specifically, the system demonstrated the ability to predict accommodation within an accuracy of 0.22 D when a subject-specific analysis scheme was employed and 0.40 D with the LOSO-CV method after two-point calibration across different subjects. Rather than evaluating the individual datasets only once, as in the subject-specific analysis, LOSO-CV analysis evaluated the same dataset a number of times equal to the number of subjects, while the split differed according to the subjects in each evaluation.

The application of the leave-one-subject-out cross-validation (LOSO-CV) methodology further strengthened the robustness and general applicability of the model. This technique ensured that the developed system could reliably perform across a diverse population, an essential feature for clinical diagnostic tools that must cater to varied individual characteristics and conditions.

Beyond the technical achievements, the practical implications of this research are vast. This technology has potential applications in fields ranging from vision research to the development of near-eye displays (NEDs), such as augmented reality (AR) and virtual reality (VR) systems. In these areas, accurate eye tracking and measurement are crucial for reducing the vergence-accommodation conflict (VAC), a common source of user discomfort. By aligning visual displays more closely with the user's natural eye mechanics, this technology can enhance the immersive experience and comfort in AR and VR environments, potentially leading to broader adoption and technological advancement in these fields.

The findings in this thesis create opportunities for further investigation into dynamic eye measurement systems and present significant prospects for commercial applications. Since our method is adaptable and highly accurate, it can be integrated into existing eye-tracking systems or developed as a standalone product for both clinical and industrial purposes. These advancements could greatly change the way we monitor, diagnose, and treat visual health.

In conclusion, this thesis presents a new approach to the measurement of eye accommodation and vergence. The integration of optical measurements with machine learning has not only addressed significant limitations of previous systems but also provided a foundation for the future. Continued development and integration of this technology could lead to significant improvements in both healthcare diagnostics and interactive technological systems.

BIBLIOGRAPHY

[1] S. R. Bharadwaj, "Accommodation mechanisms," in *Handbook of Visual Optics,* Volume One, CRC Press, 2017, pp. 363–376.

[2] R. F. Fisher, "The ciliary body in accommodation," *Transactions of the Ophthalmological Societies of the United Kingdom*, vol. 105, no. Pt 2, pp. 208–219, 1986.

[3] B. Gilmartin, "A review of the role of sympathetic innervation of the ciliary muscle in ocular accommodation," *Ophthalmic and Physiological Optics*, vol. 6, no. 1, pp. 23–37, 1986.

[4] H. Von Helmholtz and J. P. C. Southall, "Mechanism of accommodation," *Helmholtz's Treatise on Physiological Optics*, J. P. C. Southall, Ed., Trans. from the 3rd German ed. Optical Society of America, pp. 143-172, 1924.

[5] H. Martin, R. Guthoff, T. Terwee, and K. Schmitz, "Comparison of the accommodation theories of Coleman and of Helmholtz by finite element simulations," *Vision Research*, 45 (22), pp. 2910–2915, 2005.

[6] Grzybowski A, Ruamviboonsuk V. Pharmacological Treatment in Presbyopia. *J. Clin Med.*, 11 (5), pp. 1385, 2022.

[7] A. P. A. Beers and G. L. Van Der Heijde, "In vivo determination of the biomechanical properties of the component elements of the accommodation mechanism," *Vision Research*, vol. 34, no. 21, pp. 2897–2905, 1994.

[8] M. Motlagh and R. Geetha, "Physiology, accommodation," in *StatPearls* [Internet], StatPearls Publishing, 2022.

[9] D. Atchison, *Optics of the human eye*. CRC Press, 2023.

[10] S. Reichelt, R. Häussler, G. Fütterer, and N. Leister, "Depth cues in human visual perception and their realization in 3D displays," in *Three-Dimensional Imaging, Visualization, and Display 2010 and Display Technologies and Applications for Defense, Security, and Avionics IV*, vol. 7690, Issue May 2010, p. 76900B.

[11] Cleveland Clinic, "Convergence Insufficiency,"

https://my.clevelandclinic.org/health/diseases/17895-convergence-insufficiency,

Accessed: 27/04/2024, Reviewed: 06/13/2023.

[12] C. M. Schor, "A dynamic model of cross-coupling between accommodation and convergence: simulations of step and frequency responses," *Optometry and Vision Science*, vol. 69, no. 4, pp. 258–269, 1992.

[13] K.-I. Tsutsui, M. Taira, and H. Sakata, "Neural mechanisms of three-dimensional vision," *Neuroscience Research*, vol. 51, no. 3, pp. 221–229, 2005.

[14] D. M. Hoffman, A. R. Girshick, K. Akeley, and M. S. Banks, "Vergence-accommodation conflicts hinder visual performance and cause visual fatigue," *Journal of Vision*, vol. 8, no. 3, p. 33, 2008.

[15] T. Shibata, J. Kim, D. M. Hoffman, and M. S. Banks, "Visual discomfort with stereo displays: effects of viewing distance and direction of vergence-accommodation conflict," in *Stereoscopic Displays and Applications XXII*, vol. 7863, pp. 222–230, 2011.

[16] J. Geng, "Three-dimensional display technologies," *Advances in Optics and Photonics*, vol. 5, no. 4, pp. 456–535, 2013.

[17] L. Onural, "Holographic True-3D Displays: Basic Principles," September 2016.

[18] F. O. Ozhan, U. Aygun, A. Sahin, and H. Urey, "Dynamic accommodation measurement using Purkinje reflections and machine learning," *Scientific Reports*, vol. 13, no. 1, p. 21625, 2023.

[19] M. Moshirfar, R. N. Hoggan, and V. Muthappan, "Angle Kappa and its importance in refractive surgery," *Oman journal of ophthalmology*, vol. 6, no. 3, pp. 151-158, 2013.

[20] T. Eto et al., "A Purkinje image-based system for an assessment of the density and transmittance spectra of the human crystalline lens in vivo," *Scientific reports*, vol. 10, no. 1, p. 16445, 2020.

[21] M. Gneo, M. Schmid, S. Conforto, and T. D'Alessio, "A free geometry model-independent neural eye-gaze tracking system," *Journal of neuroengineering and rehabilitation*, vol. 9, pp. 1-15, 2012.

[22] T. N. Cornsweet and H. D. Crane, "Accurate two-dimensional eye tracker using first and fourth purkinje images," *JOSA*, vol. 63, pp. 921–928, 1973.

[23] H. D. Crane and C. M. Steele, "Accurate three-dimensional eyetracker," *Appl. Opt.*, vol. 17, pp. 691–705, 1978.

[24] Itoh et al., "Monocular focus estimation method for a freely-orienting eye using purkinje-sanson images," in *2017 IEEE Virtual Reality (VR)*, pp. 213–214, IEEE, 2017.

[25] C. Lu et al., "Improved vergence and accommodation via purkinje image tracking with multiple cameras for ar glasses," in *2020 IEEE International Symposium on Mixed and Augmented Reality (ISMAR)*, pp. 320–331, IEEE, 2020.

[26] J. W. Lee et al., "3d gaze tracking method using purkinje images on eye optical model and pupil," *Opt. Lasers Eng.*, vol. 50, pp. 736–751, 2012.

[27] D. Barnes and W. McDonald, "The ocular manifestations of multiple sclerosis. 2. Abnormalities of eye movements," *J. Neurol. Neurosurg. Psychiatry*, vol. 55, pp. 863, 1992.

[28] A. Serra, C. G. Chisari, and M. Matta, "Eye movement abnormalities in multiple sclerosis: Pathogenesis, modeling, and treatment," *Front. Neurol.*, vol. 9, pp. 31, 2018.

[29] T. J. Crawford, L. Henderson, and C. Kennard, "Abnormalities of nonvisually-guided eye movements in Parkinson's disease," *Brain*, vol. 112, pp. 1573–1586, 1989.

[30] E. Pretegiani and L. M. Optican, "Eye movements in Parkinson’s disease and inherited parkinsonian syndromes," *Front. Neurol.*, vol. 8, pp. 592, 2017.

[31] R. V. Kenyon, K. J. Ciuffreda, and L. Stark, "Dynamic vergence eye movements in strabismus and amblyopia: Symmetric vergence," *Investig. Ophthalmol. Vis. Sci.*, vol. 19, pp. 60–74, 1980.

[32] E. Niechwiej-Szwedo, M. Chandrakumar, H. C. Goltz, and A. M. F. Wong, "Effects of strabismic amblyopia and strabismus without Amblyopia on visuomotor behavior, I: Saccadic eye movements," *Investig. Ophthalmol. Vis. Sci.*, vol. 53, pp. 7458–7468, 2012.

[33] L. Dell’Osso, G. Gauthier, G. Liberman, and L. Stark, "Eye movement recordings as a diagnostic tool in a case of congenital nystagmus," *Am. J. Optom. Arch. Am. Acad. Optom.*, 1972.

[34] C. Wall and F. O. Black, "Algorithms for the clinical analysis of nystagmus eye movements," *IEEE Trans. Biomed. Eng.*, pp. 638–646, 1981.

[35] J. L. Newman, J. S. Phillips, S. J. Cox, J. FitzGerald, and A. Bath, "Automatic nystagmus detection and quantification in long-term continuous eye-movement data," *Comput. Biol. Med.*, vol. 114, pp. 103448, 2019.

[36] S. T. Chung, G. Kumar, R. W. Li, and D. M. Levi, "Characteristics of fixational eye movements in amblyopia: Limitations on fixation stability and acuity?," *Vision. Res.*, vol. 114, pp. 87–99, 2015.

[37] F. Ghasia and J. Wang, "Amblyopia and fixation eye movements," *J. Neurol. Sci.*, vol. 441, pp. 120373, 2022.

[38] I. Gottlob and R. D. Reinecke, "Eye and head movements in patients with achromatopsia," *Graefes Arch. Clin. Exp. Ophthalmol.*, vol. 232, pp. 392–401, 1994.

[39] P. M. Allen and D. J. O’Leary, "Accommodation functions: Co-dependency and relationship to refractive error," *Vis. Res.*, vol. 46, pp. 491–505, 2006.

[40] J. C. Chen, K. L. Schmid, and B. Brown, "The autonomic control of accommodation and implications for human myopia development: A review," *Ophthalmic Physiol. Opt.*, vol. 23, pp. 401–422, 2003.

[41] F. Lara-Lacárcel, I. Marín-Franch, V. Fernández-Sánchez, R. Riquelme-Nicolás, and N. López-Gil, "Objective changes in astigmatism during accommodation," *Ophthalmic Physiol. Opt.*, vol. 41, pp. 1069–1075, 2021.

[42] J. Geng, "Three-dimensional display technologies," *Adv. Opt. Photonics,* vol. 5, pp. 456–535, 2013.

[43] D. M. Hoffman, A. R. Girshick, K. Akeley, and M. S. Banks, "Vergence-accommodation conflicts hinder visual performance and cause visual fatigue," *J. Vis.,* vol. 8, pp. 33–33, 2008.

[44] F. Daniel and Z. Kapoula, "Induced vergence-accommodation conflict reduces cognitive performance in the stroop test," *Sci. Rep.,* vol. 9, pp. 1247, 2019.

[45] A. U. Batmaz, M. D. Barrera Machuca, J. Sun, and W. Stuerzlinger, "The effect of the vergence-accommodation conflict on virtual hand pointing in immersive displays," *Proceedings of the 2022 CHI Conference on Human Factors in Computing Systems,* pp. 1–15, 2022.

[46] 3D Consortium, "3DC Safety Guidelines for Dissemination of Human-Friendly 3D," 3D Consortium (3DC) Safety/Guidelines Section, 2010.

[47] D. M. Win-Hall and A. Glasser, "Objective accommodation measurements in prepresbyopic eyes using an autorefractor and an aberrometer," J. Cataract Refract. Surg., vol. 34, pp. 774–784, 2008.

[48] D. M. Win-Hall, J. Houser, and A. Glasser, "Static and dynamic measurement of accommodation using the grand seiko wam-5500 autorefractor," Optom. Vis. Sci. Off. Publ. Am. Acad. Optom., 2010.

[49] A. M. Gehring, J. X. Haensel, M. K. Curtiss, and T. L. Roberts, "Validation of the powerref 3 for measuring accommodation: Comparison with the grand seiko wam-5500a autorefractor," Transl. Vis. Sci. Technol., vol. 11, pp. 25–25, 2022.

[50] R. Navarro, J. Santamaría, and J. Bescós, "Accommodation-dependent model of the human eye with aspherics," J. Opt. Soc. Am. A, vol. 2, pp. 1273–1280, 1985.

[51] M. Herzberger, "Colour correction in optical systems and a new dispersion formula," Opt. Acta 6, pp. 197-215, 1959.

[52] Jaskulski, M., Marín-Franch, I., Bernal-Molina, P. & López-Gil, N. The effect of longitudinal chromatic aberration on the lag of accommodation and depth of field. *Ophthalmic Physiol. Opt.,* 36 (6), pp. 657–663, 2016.